ME3 DMT Testing and Analysis Report

E-Bike Frame

Group 1A

Mingquan Cheng
Rohhil Chhabra
Theo Hales
Zhongtian Huang
Rohit Nag

Supervisors:

Dr Li-Liang Wang
Xi Luan

Department of Mechanical Engineering,
Imperial College London

Page Count: 60
April 29th, 2021

Executive Summary

The umbrella project objective was to design, manufacture and test a fully functional electric bicycle. The project was split into sub-assemblies, with our group responsible for the main frame. In this document, the final design of the frame is revisited, its assembly and preparation for testing are explored, and the predictions for and results of this testing are explained and analysed.

We calibrated the needs of our project based on high performance, cost efficient and structurally robust engineering design. While more advanced dynamic testing such as fatigue and impact resistance was initially planned, the final testing was simplified to weighing the frame assembly and assessing resistance to static loading due to resource constraints. A light frame was deemed critical in ensuring better handling, longer range and greater portability. Withstanding static loading from 0-100 kg was critical in ensuring the frame could support the weight of an average rider (80 kg). Static loading tests were conducted using strain gauges at 5 locations, and no visible deformation of the frame was observed. The final weight of the manufactured frame was only 5.25 kg, coming in significantly lower than the CAD predicted weight of 6.103 kg and PDS specified target range of 8-14 kg. The tests were deemed successful in validating the weight and static performance criteria defined in the PDS. The loading of the frame up to and above the design load demonstrated the strength of the design and showed the trends produced by FEA predictions to be correct, which was especially impressive at a mass below the design mass of the frame. However, further testing is recommended before the e-bike can be commissioned for commercial use. Since safety is a top priority, integrity of the frame under pedalling and vibrational fatigue as well as high impact collision should be tested in the future.

Table of Contents.

Nomenclature and Abbreviations.

Symbols	Definition	Unit
ε	Strain within a component	-
σ	Stress within a component	Pa
BV	Bridge voltage (excitation voltage) applied to strain gauges	V
CI	Confidence interval	-
CNC	Computerised Numerical Control	-
E	Young's Modulus of material	Pa
FEA	Finite Element Analysis	-
GF	Gauge factor of strain gauges	-
KS/s	Kilo samples / second (sampling rate).	KS/s
n	The size of sample	-
V	Voltage measured across strain gauge during testing	V
$\bar{x}$	Mean value of the measurement data x	-
x_{lower}	Lower bound of the confidence interval of x	-
x_{upper}	Upper bound of the confidence interval of x	-
$z_{\alpha/2}$	Coefficients of confidence interval	-

Figure 1: General terminology for frame components.

1. Design and objectives overview

1.1 Report structure.

Section 1 discusses the design and the targets set for it, as well as the ways the design meets these. It also introduces any changes made since the design report submission.
Section 2 includes a review of manufactured parts – it discusses the quality of parts as assembled and any rectifying work required before testing. There is also an assessment of the quality of assembly instructions and materials supplied to the Student Teaching Workshop (STW).
Section 3 discusses the conception of tests, both those which were carried out and those which were not, and the procedures, expected and real results of the tests which were performed. It also explores the constraints and the progress of, and preparation for, the testing procedure.
Section 4 contains the group's assessment of the design in the wake of manufacture, assembly, and testing, and how this design could be improved based on these processes.
Section 5 contains the conclusions drawn from the results and assessment of the design.

1.2 Needs of the project and design suitability.

The frame of an e-bike is critical to the structural integrity of the entire system; hence the focus of this project was on high performance, cost-efficient and structurally robust design. In the initial project brief, one of the key considerations for the frame team was keeping the mass of the e-bike under 30 kg. Since the frame is the largest component of the e-bike, it was important for our team to maximise mass efficiency through effective design and space management. Having a target weight was important in ensuring portability, maximum range, and ease of handling. These needs were accounted for in the Produce Design Specification (PDS) under size, weight, and material requirements. The dimensioning of the frame considered the ergonomics associated with an average male rider. Since the mass target for the whole e-bike was 30 kg, we kept the target mass for the frame within the range of 8-14 kg. Finally, material selection was a two-fold process. The first criterion was to choose light, cost-efficient materials. The second criterion tied into the next key consideration for the frame team, which was fracture performance and damage resistance.

Figure 2: The full frame as assembled for testing.

Since the nature of the product is such that it is exposed to potentially harsh conditions, we aimed to design the frame to be environmental damage resistant as well as fatigue, impact and buckling resistant. Such characteristics were important in ensuring structural integrity in the event of an accident. While these were key design considerations, testing for all the criteria would have been too costly and time consuming. Since dynamic performance was difficult to test, we decided that the minimum performance standard that the frame should be able to withstand was static loading. While the assumption was that the average rider weighs 80 kg, we wanted the frame to be able to withstand greater static loading with a significant factor of safety. Additionally, since the e-bike was designed for urban use, it was not as critical to test for vibrational fatigue as it would be for a multi-terrain bike.

Hence, the critical elements of the PDS that were tested were the weight target and static stress performance. Since FEA was used to predict performance for all components of our frame, collecting stress and strain test data allowed us to validate our FEA models.

The greatest resource constraint in the project was cost. Hence, many design considerations were motivated by maximising cost efficiency. Several design iterations and simplifications were made to improve ease of manufacture, thus reducing cost of production. In the iterations, thin sections and precision engineering cuts were avoided as much as possible.

Additional design considerations that were non-critical yet important include user experience and ease of assembly. For comfort, in depth research was conducted on rider anatomy and ergonomics to ensure better handling for an average size male rider (169-176 cm). Finally, since

the project was split into sub-assemblies, we had a responsibility to ensure that the frame design fits well with the rest of the e-bike structure. Acting as the central component, it was important that the frame was designed in an adaptive fashion that was able to balance the needs of each sub-assembly. The dropouts were designed to fit the needs of the motor team, incorporating a tensioning mechanism while still being compatible with the disc brakes.
The final design of the frame catered to the other subassembly groups by having a box section seat tube and down tube. This aided the motor group and the battery group in attaching their subassemblies more easily, with the motor group brazing their support plate directly to the seat tube and the battery group bolting their subassembly on to the down tube. The steering assembly was integrated into the design via a custom-machined bespoke diameter head tube, which contained their headset assembly. These, along with the sliding dropouts, made the frame distinct from market models and offered easier integration to the other teams working on this project.

Table 1: Frame group Product Design Specification.

Element	Criteria	Verification	Date Modified
User Experience			
Needs	To accommodate for a comfortable ride position. Battery module must be integrated into frame.	Market Research on what is preferred and required.	05/11/2020
Market	Type of bike and specific features must fit city cycling requirements.	Research and compare to current urban, hybrid and road bikes.	05/11/2020
Physical Properties			
Size	54 cm frame designed for a rider of height (169-176 cm). Reach of approx. 380 mm and handlebar	Research average human dimensions and corresponding frame measurements.	05/11/2020

	height of approx. 830 mm.		
Weight	Overall weight range: 15-30 kg Frame weight range: 8-14 kg	Calculate material weight using overall dimensions before manufacturing. Confirm weight by weighing manufactured frame.	05/11/2020
Wheels	700cc (622 mm) Quick release mechanism.	Will be purchasing wheels. Detailed stress analysis will be performed to verify frame compatibility.	05/11/2020
Material	Must be able to withstand impact stress tests according to British standards. Must meet frame weight range. Corrosive and weather resistant.	Material Selection through CES Material Package.	05/11/2020
Cables and Wiring	Must accommodate for connections to motor and battery. Internal wiring reviewed; not employed on first iteration.	Review with drivetrain, battery, and motor team.	16/02/2021
Shape	Avoid having sharp edges and corners.	FEA analysis and design review.	05/11/2020
Saddle and seat-post	Frame must accommodate for standard 27.2 mm seat post.		05/11/2020
Fenders and mudguard.	Mudguard attachments for front were responsibility of		16/02/2021

	steering group. Rear mudguard does not need explicit attachment as it can clamp to the seat post.		
Performance			
Fatigue	Must be able to withstand cyclic forces to simulate riding conditions on the road and pedaling forces.	Testing according to (BS EN 15194:2017) sits outside of the budget of the group and specialized rigs for these tests are costly to produce and obtain. Tests also call for deformation of the frame which serves to weaken the bike; dummy component test methods will be employed. (to avoid damaging the original frame). FEA to be used to predict most vulnerable components. Verification by visual inspection of visible cracks or fractures in the assembly. There should also be no separation of parts at the joints.	26/02/2021
Impact Resistance	Must be able to withstand direct impact forces (horizontal and vertical) in cases of unnatural conditions and collisions.	Visual inspections of deflection and cracking performed under loading. FEA to be used to predict most vulnerable components.	26/02/2021
Bending, deformation and stress.	Frame must be able to support an 80 kg rider under static stresses.	Measurement of stresses required to cause complete failure of critical components taken with Instron machine. FEA modelling and stress analysis used to predict most	26/02/2021

		vulnerable components under largest stress.	
Operating Environment	-5 °C – 40 °C for wide range of cities	Select materials based on these operation temperatures.	26/02/2021
Safety factor	Frame must exhibit a safety factor of 3 under normal riding loads.	FEA modelling.	26/02/2021
Life Span			
Product Life	5 years	To be considered during material selection and calculation	05/11/2020
Service Life	10 years		05/11/2020
Production			
Quantity	10 million.	To cater for the ever-growing need for urban transportation	05/11/2020
Product Cost	4 times of manufacturing cost Market price is around £1000-£10000	Calculation of cost of material when bulk purchase, cost of manufacturing	05/11/2020
Manufacturing Cost	Price of components and material with various manufacturing methods		05/11/2020
Regulatory			
Safety Standards	Compliance to all BSI Standards	Conform to BS EN 15194:2017 where possible	05/11/2020
Environmental Impact	Sustainable materials where possible	Source sustainable materials	05/11/2020
Production Regulation	Compliance to BSI Standards	Reference to BS EN 15194:2017 – testing methods to be assessed comparable to this where possible, but see previous performance section for assessment of validity of testing to this standard.	16/02/2021

1.3 Latest design changes.

The design was heavily modified up-to the design report phase. These modifications were driven by the aim of making the frame as manufacturable and economical as possible. The design process halted with the confirmation of fabrication capability from the manufacturer. Unfortunately, the delayed quotation far exceeded the allocated budget. The approach taken to further lower the cost of manufacturing was to redesign the seat-tube and top tube intersection. The previous design of this area is shown in Figure 3. The end of the square section seat tube featured complex oblique cuts at out-of-plane angles, for slotting the seat-stays. Furthermore, the sealing top cap also featured similarly complex cuts.

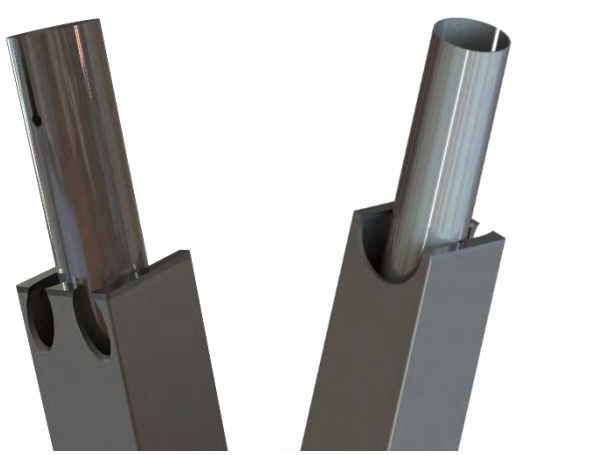

Figure 3: The previous seat tube design.

This area was heavily simplified by extended the square sectioned tube beyond the intersection point and having flat surfaces for joining tubes to weld on to. This is shown in Figure 4. The redesign was taken as an opportunity to add support ribs between the external square and internal circular seat tube. This would add resistance to warping during welding.

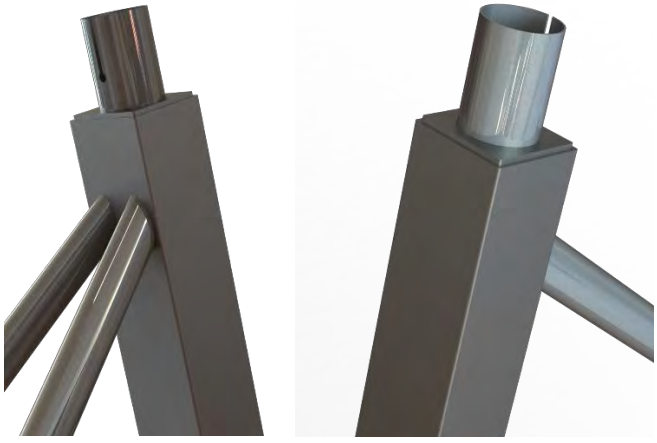

Figure 4: The redesigned seat tube with simplified cuts.

2 Review of manufactured parts and assembly

2.1 Review of manufactured parts.

The head tube became slightly deformed due to heating from the joining process when the frame was built, which resulted in it losing its concentricity. Work was required to fit the bearings in for the headtube assembly, which was achieved by pressing the head tube back into shape using the bearing housings. No other changes were required before testing. The brake discs were reported to be loose by the STW so more instruction besides the manufacturer's directions for the wheels / brakes may have been needed. This is further explored in Section 4.2.

2.2 Review of assembly.

The instructions were broadly sufficient, in so far as in photos from the STW the frame looked complete (as intended for the testing stage and according to the group's instructions), and assembly only took around half a day from delivery and reception by the stores. The full assembly is shown in Figure 5. During the assembly process, the left dropout insert was threaded by the workshop as the manufacturer was unable to thread the hole as required. This was required to secure the thru axle, and without this addition the rear wheel assembly would not have functioned as intended. This was achieved without incident with the engineering drawings having been supplied to the workshop. The frame was joined as specified by the manufacturer and looked as expected (with access, measurements would have been taken to confirm details such as the placement of the motor plate or battery bolt holes). With this not being possible, though, the images sufficed. There were no pressing difficulties with the assembly process due to the assembly itself, nor was the group notified by the manufacturer of any problems. No modifications to the frame were required before it was ready for testing.

Figure 5: The frame and steering fork assembled for testing.

However, there were some issues during the assembly process which might have been avoided. There was some confusion regarding the location of the axles, which led to the front and back axles needing to be switched such that the aluminium rear thru-axle (designed by the group) was in the correct place and could screw into the left side threaded nut. This could have been rectified with clearer instruction or perhaps an additional view of the rear axle and left side nut assembly specifically, demonstrating that the threads should interlock. The aluminium axle should have been in the rear wheel but was left at the front (as shown in Figure 6) until the STW staff were instructed to rectify it.

Figure 6: The frame with the Aluminium thru-axle as designed by the group in the front wheel.

It is likely that had the group had access to the workshop and been able to assemble the frame, these issues could have been mitigated or might not have arisen (specifically the axle could have been placed correctly). However, the instructions provided for the assembly could have more clearly reflected this in the first place. It was also discovered that, as shown in Figure 5 and Figure 6 above, the wheels which were purchased did not come with tyres as had been shown on the website. This was not checked as the group was working on finalising other orders and the design report, quality plan and test preparations and did not have access to the stores or STW to look at the parts. It should have been more carefully confirmed during ordering but was rectified easily and tyres were sourced within budget and fitted to the wheels prior to testing. Initially, the intention was to improve aesthetics of the frame and cover the heat marks from the joining process by painting the frame. However, this would have interfered with the strain gauge adhesion for testing so was not completed. Additional time and cost savings resulted from this decision.

The testing assembly only required the saddle and wheels, and steering assembly be provided. Due to delays with the manufacture and shipping of the frame, testing commenced close to the

deadline and there was insufficient time to assemble the full frame with all its components, as groups were focused on preparing for the final deliverables of the project.

3 Description of testing

3.1 Test generation.

Multiple iterations of testing plan were made mainly due to strict budgeting and availability of testing machines. Because of the global covid pandemic, testing resources across all engineering departments were limited, with some only available to their domestic PhD students. In addition, the shortage of testing resources also influenced the choices of test as those with a long duration (fatigue tests for example) were unfeasible.

Initial tests were devised based on the tests described in the British Standard for Electrically Power Assisted Cycles (EPACs). These were chosen to validate the integrity of the frame and are shown in Table 2 below.

Table 2: Test descriptions. (Hales, Nag, Chabra, Cheng, & Huang, 2021)

Test Name	Required Resources	Test Personnel	Test Facility	Test Date	Test Duration	Priority Level	PDS Criteria
1. Frame Impact Test (Falling Mass)	Striker of Mass 22.5 kg, Roller of Mass <= 1 kg, Rigid mounting for rear axle attachment point, Dummy Fork	1 x Technician	STW	15th March 2021	10 mins	High	Performance - Impact Resistance
2. Frame Impact Test (Falling Frame)	30 kg, 10 kg, 50 kg masses, Steel Anvil (A flat platform), Roller of Mass <= 1kg, Rigid mounting for rear axle attachment point, Dummy Fork	1 x Technician	STW	15th March 2021	10 mins	High	Performance - Impact Resistance

3. Frame Fatigue Test (Pedalling Forces)	Rigid mounting (of height = radius of the wheel/tyre assembly ± 30 mm) for fork axle attachment point, Stiff vertical rod/link with ball-jointed end	1 x Technician	STW	15th March 2021	3 hours (100,000 cycles at 10Hz)	High	Performance - Fatigue
4. Frame Fatigue Test (Horizontal Forces)	Free-running channel guided roller for front axle Rigid, pivoted mounting for rear axle attachment point	1 x Technician	STW	15th March 2021	3 hours (100,000 cycles at 10Hz)	High	Performance - Fatigue
5. Frame Fatigue Test (Vertical Forces)	Free-running roller for front axle, Cylindrical steel bar (dummy seat post), Rearward extension bar (horizontally attached to dummy post), Rigid, pivoted mounting for rear axle attachment point	1 x Technician	STW	15th March 2021	1.5 hours (50,000 cycles at 10Hz)	High	Performance - Fatigue
6. Functional Deformation Impedance Test	Full bicycle assembly 200 kg load	1 x Technician	STW	15th March 2021	30 mins	Low	Performance – Bending, Deformation and Stress
7. Purchased Components Manufacturing Specification Verification	Seat Post + Saddle Wheel + Tire	1 x Technician	STW	15th March 2021	30 mins	Low	N/A

Details of the five high-priority tests can be found in Section 3.7.

The testing plan was proposed given a strict budget and limited access to facilities. This was called the second iteration since the initial considerations were the use of the British Standard tests. Three options were considered to preserve the original frame's integrity.

1. **Dummy Component Testing:** Destructively testing the selected components identified to be under increased stress. Individual substructures would be manufactured separately and then tested.
2. **Non-destructive Testing:** Test the complete frame at loads below failure values to avoid damage, obtaining strain data using strain gauges.
3. **Fracture Modelling:** The complete frame would be loaded until crack initiation, then fracture mechanics methods would be used to calculate the conditions for crack propagation.

A testing decision matrix, Table 3, was made in order to select the preferred alternative method:

Table 3: The matrix of available tests. (Hales, Nag, Chabra, Cheng, & Huang, 2021)

Test Name	Pros	Cons
1. Dummy Component Testing	• Models the stress concentrations well • Can be tested destructively • Does not require the large and complex rigs that a full frame assembly would require • Protects original frame from any damage • Cheapest option • Easiest testing method	• Relies on FEA modelling to identify highest stress components • Requires brazing and cutting to replicate similar stress concentrations • Not a test of the full frame assembly • Requires additional manufacturing and material
2. Non-destructive Testing	• Protects original frame from significant damage • Saves costs associated with destructive dummy component testing • Tests the full frame	• Introduces no failure in the frame • Overly reliant on calculations and models • If FEA models are not accurate, risk of accidental and irreversible damage to original frame • Difficult to define fraction of stresses to be applied • Requires as many testing resources as iteration 1

3. Fracture Modelling	• Does not require additional components for fully destructive testing • Introduces some failure which allows for a higher safety factor than non-destructive testing • Tests the full frame	• Damages original frame • Fracture modelling cannot fully replicate real crack propagation, which can be affected by additional thermal or residual stresses that are difficult to model • Requires as many testing resources as iteration 1

Dummy Component Testing was selected from the matrix as it not only protects the original frame while receiving accurate testing results, but also lowers the overall cost to meet the tight budget constraints. In total, two methodologies of dummy component tests were considered. The first one contains five dummy component tests transformed from the British Standards while minimising the number of additional components and testing rigs required, and the second one would conduct all five tests on a dummy rear triangle from the bike frame. As a result, the frequency, number of cycles and forces have been kept the same. Additionally, all striker masses and impact forces were kept at similar values. These tests were designed to be a decomposed version of the full frame tests, to enable them to be performed with the equipment available at the college rather than specialised testing rigs designed for bicycle frames. This is explained further in Section 3.7. The standard tests on which the dummy component tests were based, and which influenced the first iteration of the testing process, can be found in BS EN 15194:2017 (BSI, 2017), under section 4.3 Mechanical requirements, on pages 53-59.

As mentioned in the beginning of this section, dynamic tests in general were impractical due to limitations on time and testing resources. Therefore, the remaining tests were the box section seat tube buckling and top tube impact fracture tests. In addition, the department did not approve extra funding for dummy components. All of these factors eventually made the frame team transfers from dummy component testing to non-destructive testing. Based on research for non-destructive tests of bike frames, some preliminary tests like visual inspection of possible cracks on bike tubes and tap tests can be conducted in the lab. For the tap test, the inspector would listen for any audible change in pitch and resonance as an implement moved along the frame. However, this requires years of expertise in the frame building industry therefore it is anticipated that not much information can be gathered with this test. Techniques using thermographic or radioactive to detect internal cracks could be useful but were not available at

the department. Eventually, the frame team decided to only conduct static loading tests on the full frame.

3.2 Specification.

3.2.1 Static load test.

The specification used for this test was as follows: a threaded bar was to be placed across the saddle, with two nuts on each side used to locate and constrain the hangers for the masses, which would hook on to the bar. The mass applied to the saddle would be increased in 20 kg intervals from 0 kg up to 60 kg, and then in 5 kg increments up until the maximum load of 100 kg. This ensured that the loading could be increased faster when the mass was less critical and then at the more sensitive region, around the average mass of a rider (assumed to be 80 kg), the addition of mass slowed down both to gather more data for different loads but also to ensure that the frame was not loaded too quickly and thus damaged. (More gradual increases at higher masses would allow for any damage to be spotted before it became too serious. The frame was supported at the rear wheel, and the masses were loaded at the saddle since the test was concerned with the use case of a sedentary rider, and the front fork had already been tested by the steering team, so the focus was on the performance of the frame.

A combination of 0-90 T-shaped and linear strain gauges were used, with the linear strain gauges at sites where stress was less concentrated and the 0-90 gauges where there was particular interest in strain values. Initially, strain gauge rosettes were specified, but the department did not have these available and the group did not have the budget or time to procure them, so linear gauges in a single and 0-90 configuration were used instead.

The load limit of 100 kg was employed to ensure performance even above the specification rider weight of 80kg. This enabled the integrity of the frame to be proven, since 80 kg is an average figure and not representative of the entire population that might use the bike. Furthermore, in previous simulations and in Figure 7, the safety factor was shown to be lower, around 1.1.

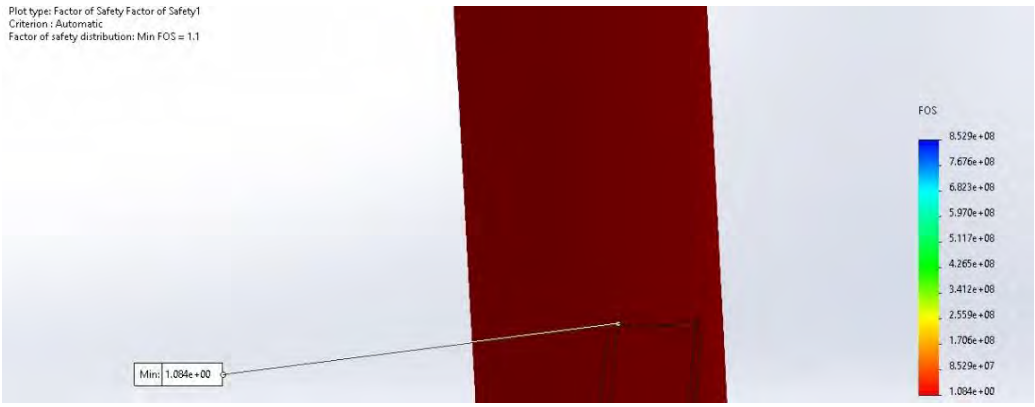

Figure 7: The minimum safety factor of a previous analysis of the frame. *(Hales, Nag, Chabra, Cheng, & Huang, 2021)*

This was below the PDS value of 3, as discussed in the design report, so testing at higher loads was employed to increase confidence in the design.

Strain values were added, from the FEA simulation, to provide limiting values for the strain during the experiment. These, along with the full testing specification used for this test, are shown in Section 3.2.2.

3.2.2 Static load test plan – full.

Equipment required:

- Frame (assembled with rear wheel)
- Front fork and handlebars, assembled with front wheel and attached to frame
- Bicycle stand / support
- Masses up to 100 kg total and their hangers (x2)
- Strain gauges and reader (6x strain gauges, four arranged as two linear 0-90 T shapes, and two linear)
- Threaded bar, 500 mm
- M8 nuts x 4
- M8 washers x 4
- Cable / metal ties x 8
- Electrical tape

Setup:

Ensure bike is assembled with strain gauges attached as per the diagram and secured in the bike stand such that the bike is balanced vertically and does not rock or wobble.

0-90 strain gauges should be applied as per the diagram, as well as axially oriented halfway along the length of the top tube, and axially oriented halfway along the downtube, as per the diagram.

Electrical tape should be used to cover the central thread where the bar meets the saddle to avoid damage to the saddle itself.

Nuts should be screwed on such that the hangers sit 145 mm from the centre of the saddle or 5 mm in from the end of the 300 mm bar. This should provide 30 mm clearance between the masses and the outside of the seatpost tube.

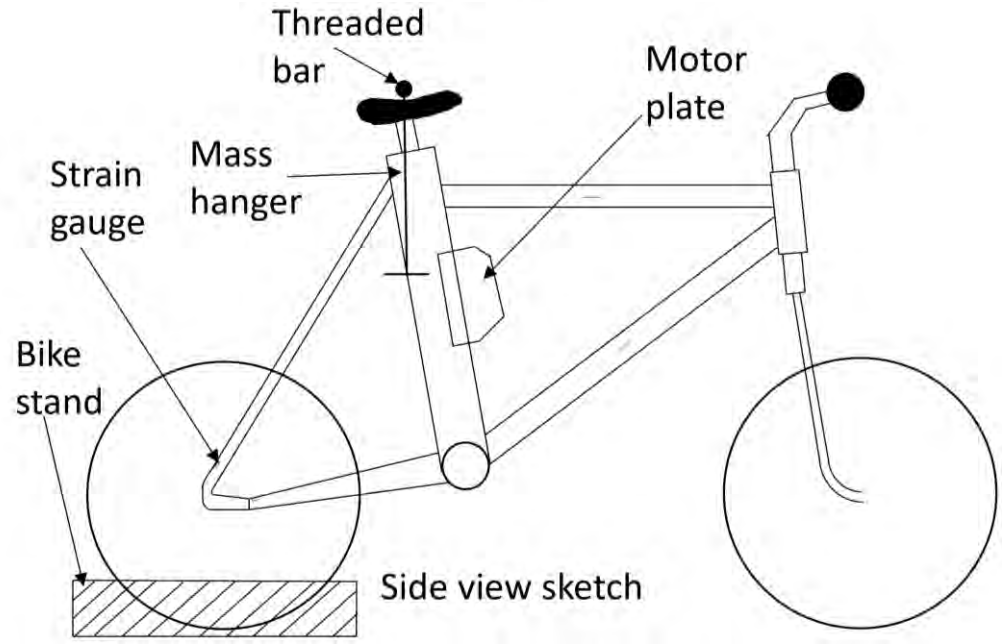

Figure 8: Side view of bike in stand showing strain gauge placement.

= 0-90 strain gauge.

= single strain gauge.

Figure 9: Strain gauge key.

Test method:

Apply masses starting from 0 up to 100 kg in increments of 20 kg, up until 60 kg, at which point, mass should be increased in 5 kg increments until 100 kg.

Once mass has been applied, allow strain gauge readings to settle before recording strain values at each load. Take 3 readings for each load.

The masses should be applied to their hangers, which are suspended from a threaded bar atop the saddle, which is secured to it and has nuts wound onto the ends to prevent the hangers from sliding off – see Figure 10.

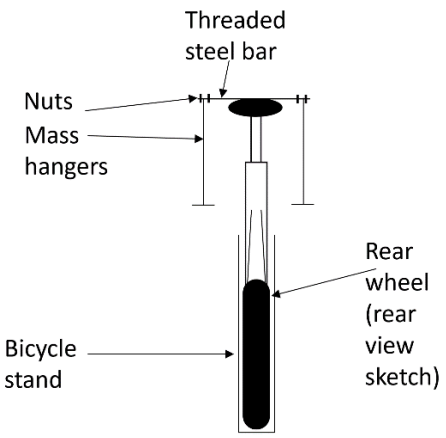

Figure 10: Rear view of bike in stand loaded with masses.

Ensure during loading that deformation is not excessive (to prevent damage to the frame, which would cause other groups to be unable to mount their components). The frame should also not contact the wheels at any point during tests. If this occurs, the load and the strain values at which contact happens should be noted, and further loading should be stopped. Limiting strain values for each load are displayed here and have been calculated from FEA performed on the frame at the masses specified for testing. They serve as cautionary values but any visible cracking or damage to the frame should cause any further loading to be stopped and the conditions where the damage was noticed should be recorded.

These strain values are tabulated below according to the applied mass and their component.

Table 4: Strain gauge number, position and predicted values.

Component	Strain gauge number	Limiting strain value (100 kg)	
		Max	RMS
Axially oriented, inner seatstay (0°)	1	9.645×10^{-5}	7.381×10^{-5}
Hoop oriented, inner seatstay (90°)	2	1.145×10^{-4}	7.155×10^{-5}
Axially oriented, inner chainstay (0°)	3	6.356×10^{-5}	6.088×10^{-5}
Hoop oriented, inner chainstay (90°)	4	6.324×10^{-5}	5.741×10^{-5}
Axially oriented, top tube	5	3.331×10^{-6}	2.772×10^{-6}
Axially oriented, downtube	6	1.086×10^{-5}	1.076×10^{-5}

Since the elements used in FEA were on the order of 3 mm in size, the area covered by the strain gauge in use would take up multiple elements. As such, the strain gauges would be reading in effect an 'average value' on the frame, and so a locus of elements on each component in the position of the strain gauge was used, to provide more accurate strain values in these areas. The images from FEA which show the elements used to derive these values are shown in Appendix 7.1.

Below (Figure 11) is an image of the frame during strain gauge attachment for testing.

Figure 11: Image of the frame during strain gauge welding, showing strain gauge sites.

3.2.3 Weighing.

Additionally, the frame was weighed upon arrival at the Stores to assess its mass compared to the PDS weight range and the prediction made by the CAD model. This was to ensure that it met the weight target as set by the group at the start of the project, whilst the load test would determine whether the frame was sufficiently strong under the weight of a rider.

The Stores staff were asked to weigh the frame (along with the dropout inserts and axle; so, the total working mass of the frame minus wheels and saddle) when it was received, since the STW did not have the facilities to carry this out.

3.3 Expected results.

3.3.1 Static load test.

FEA was performed on a CAD model of the frame to assess the stresses and strains present within it, and to ensure that the frame was acceptably strong at its design rider mass of 80 kg.

The predictions from this FEA are shown below, and the tabulated data from which these were plotted is displayed in Appendix 7.1.

The frame was not expected to deform much, shown by the low values of the strains obtained in each component and at the sites of the strain gauges. The high safety factor and low stresses indicating this are shown in Figure 12 (a) and (b) and Figure 13 (c-f).

The strain values produced by the analysis were absolute.

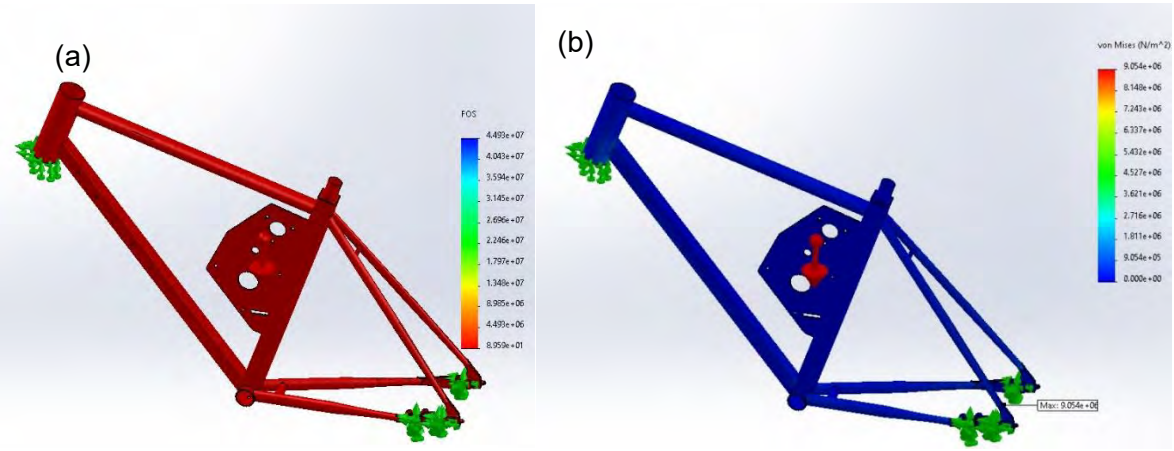

Figure 12: Plots of the frame showing both minimum Safety Factor (a) and von Mises' equivalent stress (b) at 0 kg.

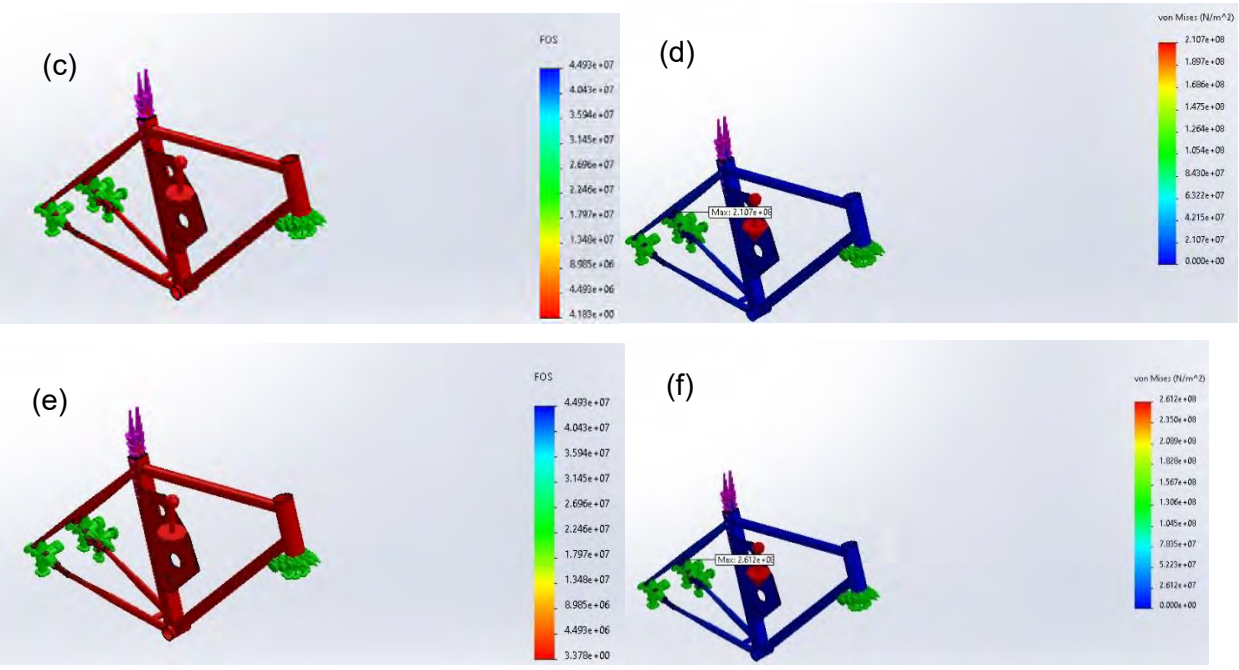

Figure 13: Plots of the frame showing both minimum Safety Factor (c, e) and von Mises' equivalent stress (d, f) at 80 and 100 kg.

The minimum safety factors of 90 at 0 kg, 4 at 80 kg and 3.4 at 100 kg show the strength of the frame under the weight of the rider. The maximum stresses are shown on each of the von Mises plots, to be 9.054 MPa at 0 kg load, 210.7 MPa at 80 kg load, and 261.2 MPa at 100 kg load.

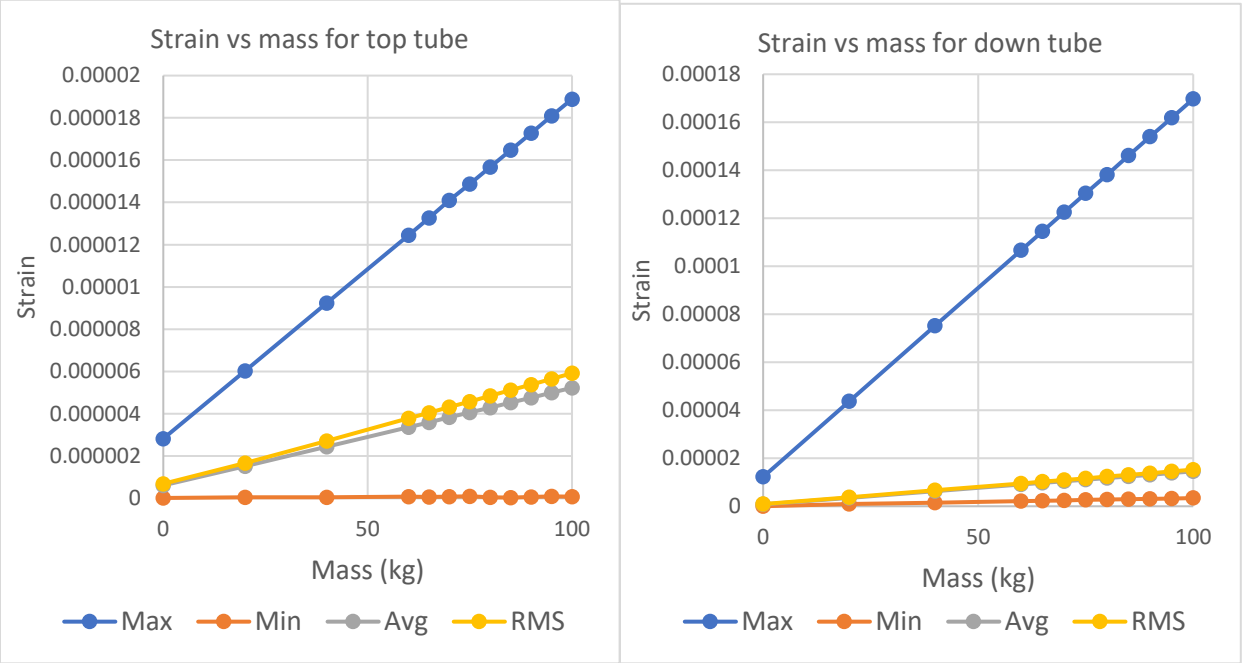

Figure 14: A plot of strain vs applied mass on the frame at the top tube and downtube, as predicted by FEA.

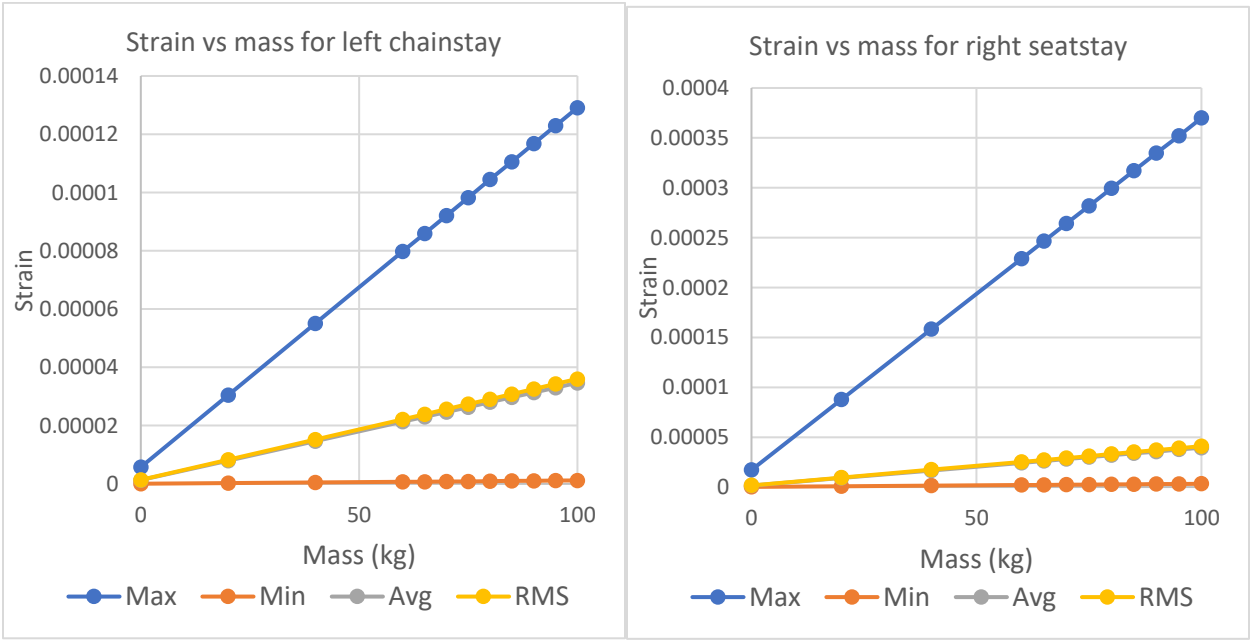

Figure 15: A plot of strain vs applied mass on the frame at the left chainstay, and right seatstay, as predicted by FEA.

From these graphs, a linear relationship between the mass applied and the strain in these components is expected. This makes sense, as force is directly proportional to stress, and stress is directly proportional to strain. Thus, as long as the material remains within the linear elastic region (which is assumed in general), this relationship will hold for all components of the frame under loading. To validate the data obtained from the simulations, strain gauges were placed both at locations of interest and further away, where increased strain was not expected. For example, strain gauges were placed near the dropout joint on the chainstay, and near the dropout join on the seatstay. For additional comparison, strain gauges were also positioned at remote locations on the top tube and downtube (axially oriented halfway along their length), far from any joins.

As well as the strain values being recorded and compared, the frame should not contact the wheels at any point under loading. This would obviously hinder the rideability of the bicycle and could also potentially cause damage to the wheels, drivetrain, or axles. The frame contacting the wheels would be considered a failure to support the load on it at this point, which might affect the overall validity of the frame design, depending on whether this occurred below or above the design weight of 80 kg. The frame would be judged successful if it could support the prescribed loads without touching the wheels or excessively deforming, and it should also conform to the predictions made by FEA (although exact agreement is not essential, since very precisely or perfectly modelling the frame and its behaviour would be extremely difficult).

Since the values displayed above were taken from each component in the simulation, rather than a specific area, more data had to be gathered to check the average values given by the strain gauges. The principal strain values were taken from the FEA at the positions of each strain gauge, at loading of 100 kg, to provide limiting values for the test. These are discussed in Section 3.2.2.

The effects of gravity were also included in the simulation, both to demonstrate that the frame could support its own mass (giving a maximum stress as shown on the order of 9 MPa and a safety factor of 90, in the simulation without any load present on the frame).

The graphs above (Figure 14 and Figure 15) show that the strain values are expected to be highest in the seatstay, then the downtube, then the chainstay and then the top tube. This can be explained by the significant stress concentration factors within the seatstay and chainstay (in the case of the cut to accommodate the dropout), and also in the downtube in the case of the bolt holes drilled to accommodate the battery. The fact that the downtube separates the two dropout attachment points is curious since the seatstay and chainstay have stress concentration factors of a similar nature, so one might expect their values to be sufficiently similar that they

would both be the highest or second highest in this list. However, as can be observed both from the graphs and from Table 4, the difference in size of these values is very small, as they are of the same order (or similar orders) of magnitude, so there is some probability that a more accurate finite element model would uncover whether the values are in fact so closely grouped, or whether greater resolution is required to explore the exact relationships between the values.

3.3.2 Weighing.

The expected value for the frame from the PDS was between 8 and 14 kg. This was to keep the overall weight of the full bicycle below 30 kg, with the expected values for the full assembly to be between 15 and 30 kg. At the time of writing, assembly and weighing of the full bicycle had not been planned as part of the testing.

From the SolidWorks model of the frame, the mass of the frame was predicted to be 6.013 kg. This was lower than the PDS value, and provided a current estimate of the mass of the frame. These values were not prescriptive, so the weight being below them would not constitute a failure of the frame, but the weight being higher than the 14 kg maximum value would. This test would lend further confidence to the design in conjunction with the previous, since the frame being at (or below) its target weight while still providing sufficient strength would represent a successful (or indeed very successful) design. If the frame is above its target weight, the strength of the design is important but is also then impacted by the lack of an important design criterion since the overall bike would be overweight.

3.4 Results.

3.4.1 Static load test.

During the preparation for testing, soldering caused one of the strain gauges which had already been attached to the frame to break. With more time and access to the frame, the group would have liked to replace this strain gauge to ensure the full range of data was available, but this was not possible due to the nature of the project, so the test proceeded with five strain gauges in use. The strain gauge which was damaged was number 4 and was situated on the chainstay, oriented in the hoop direction.

The equipment used for monitoring and recording the strains during the test is described as follows. The strain gauges used were the 120LZ and 240UZA gauges from Micro-Measurements. The data acquisition system used was the Fylde Micro Analog 2 FE-MM16, using FE-366-TA bridge transducer amplifiers, and the software used was Madaq 16.

The data recording was intended to be performed with a 1 KS/s sampling rate, and the load was to be left at each value for 30 seconds to allow the readings to settle and the increase in loading to be prominent. This was not achieved, so instead images were taken of the voltage readings at each applied mass on the frame and were subsequently copied out from the images for analysis. The strain gauge position and channel numbers are related to their number in the test specification and displayed in Table 5 below.

Table 5: Strain gauge positions, numbers and channel numbers.

Strain gauge number (as per test specification)	Strain gauge location	Channel number	Gauge type
5	Top tube	1	240UZA
6	Down tube	2	240UZA
2	Seatstay, hoop oriented	3	120LZ
1	Seatstay, axially oriented	4	120LZ
3	Chainstay, axially oriented	5	120LZ
4	Chainstay, hoop oriented	Damaged, not used.	120LZ

The test was carried out by Joseph Terry, a Graduate Teaching Assistant (GTA). The group was put in touch with him by Dr Ruth Brooker after submitting testing requirements.

The test proceeded well, until the mass reached 40 kg. At this point, the rod supplied to support the hangers was not fit for purpose and began to severely deform so a new, thicker rod was sourced and attached to the saddle in its place. It is worth noting that the original 300 mm long rod supplied in the test specification was not long enough to support the mass hangers whilst providing adequate clearance to the frame, so this was replaced by a longer bar once a new requisition form had been submitted to the stores, which was then again replaced by the necessary thicker rod. The mass of this rod was 2.77 kg, and the mass of each hanger was 1 kg. The strain gauges were zeroed (or ‘balanced’) with these already applied to the frame so they were not accounted for in the overall mass placed on the frame during testing.

The loading then resumed, and continued up to 90 kg, at which point the stand began to deform under the force exerted by the rear wheel of the bicycle leaning against it, and could no longer

reliably hold the bike vertically steady. Loading was stopped at this point, so data was acquired up to a mass of 85 kg instead of the full 0-100 kg range.

However, the frame did not deform excessively or exhibit excessive damage during the test, shown by the GTA being able to continue loading it until testing had to be stopped due to the stand. Furthermore, as shown in Figure 16 below, the testing setup of the bike looks very similar to the test diagram as in the specification in Figure 8.

The results of the tests were taken from the voltage values displayed on the Madaq readout, Figure 16, and these voltages are tabulated in Appendix 7.2.

Figure 16: The bike as set up for testing with the Madaq voltage values on the screen.

The voltage readings were then converted into strain readings using the equation $\varepsilon = \frac{4V}{BV \times GF}$ (National Instruments, 1998), and are collected in Table 6 below.

Table 6: Strain readings for each component at each mass.

Mass (kg)	Channel	Component	Strain 1	Strain 2	Strain 3	Strain 4
0	1	Top tube	0.006667	-0.00039		

0	2	Downtube	0.004314	0		
0	3	Seatstay hoop	0.002667	0.002667		
0	4	Seatstay axial	0.003048	0.001143		
0	5	Chainstay axial	0	0.00381		
20	1	Top tube	-0.00078	0.001176	-0.00157	0.001176
20	2	Downtube	0.001961	0.002353	0	0.002353
20	3	Seatstay hoop	0.006095	0.005333	0.006476	0.005333
20	4	Seatstay axial	-0.00152	0.000762	-0.00076	0.000762
20	5	Chainstay axial	0.010286	0.010286	0.01219	0.010286
40	1	Top tube	-0.00588	-0.00392	-0.00471	
40	2	Downtube	0.001176	0.001176	0.001176	
40	3	Seatstay hoop	0.006476	0.008381	0.006476	
40	4	Seatstay axial	-0.0061	-0.00495	-0.00495	
40	5	Chainstay axial	0.019048	0.01981	0.018286	
60	1	Top tube	-0.00902	-0.00941	-0.00902	
60	2	Downtube	0.002745	0	0.000784	
60	3	Seatstay hoop	0.005714	0.004952	0.00381	
60	4	Seatstay axial	-0.00305	-0.00152	0.000381	
60	5	Chainstay axial	0.026286	0.026667	0.027048	
65	1	Top tube	-0.00549	-0.01059		
65	2	Downtube	0.004706	0		
65	3	Seatstay hoop	0.004571	0.00381		
65	4	Seatstay axial	0.001524	0		
65	5	Chainstay axial	0.027429	0.02819		
70	1	Top tube	-0.0098	-0.01216		
70	2	Downtube	0.002745	0.000784		
70	3	Seatstay hoop	0.00419	0.00381		
70	4	Seatstay axial	-0.00038	0		
70	5	Chainstay axial	0.030857	0.030857		
75	1	Top tube	-0.01137	-0.0098	-0.01137	
75	2	Downtube	0.001176	0.001961	0.000784	
75	3	Seatstay hoop	0.002667	0.003429	0.002667	
75	4	Seatstay axial	0.002667	0.00381	0.004571	
75	5	Chainstay axial	0.033905	0.033524	0.033143	
80	1	Top tube	-0.01294	-0.01294	-0.01176	
80	2	Downtube	0.000392	0.002353	0.004706	

80	3	Seatstay hoop	0.001524	0.000762	-0.00038	
80	4	Seatstay axial	0.003429	0.004952	0.005333	
80	5	Chainstay axial	0.041143	0.041524	0.039619	
85	1	Top tube	-0.01412	-0.01373		
85	2	Downtube	0.001961	0		
85	3	Seatstay hoop	-0.00267	0		
85	4	Seatstay axial	0.009905	0.011429		
85	5	Chainstay axial	0.044952	0.045714		

For some of the masses, only two readings were taken from the Madaq software readout, whereas at other loads, there were three or four. Three readings per load were requested, but there was no time after receiving the data to rectify some data points having fewer than this. These strain readings were averaged for each component at each load, and an additional average was calculated using the average voltage at each strain gauge site for each load. The plots are displayed in Figure 17, Figure 18, and Figure 19 below.

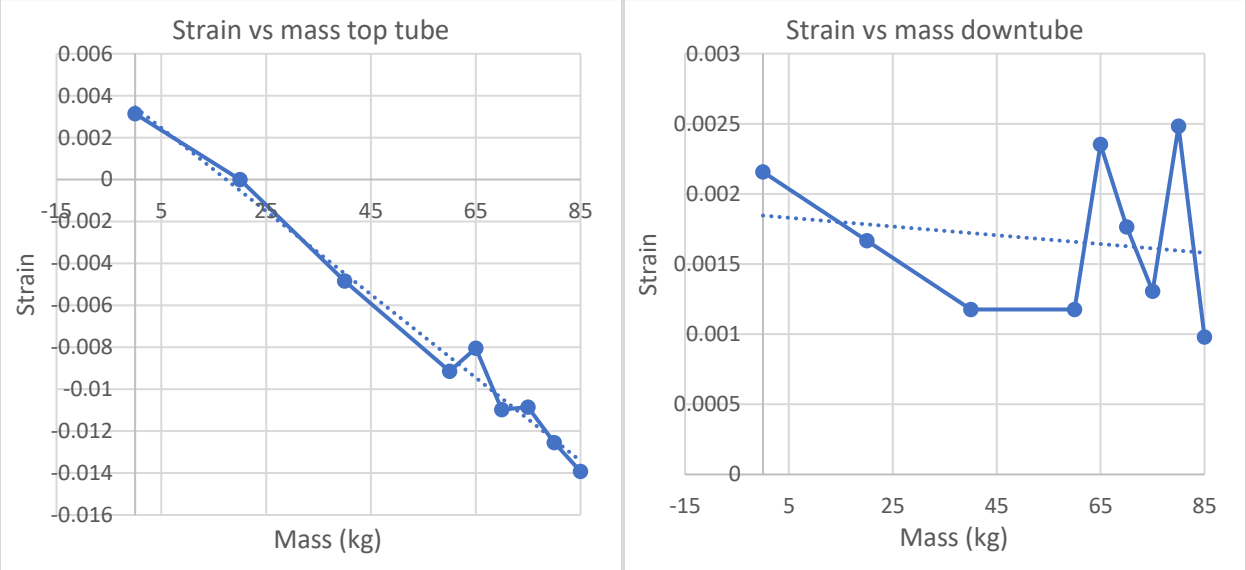

Figure 17: Plots of the strain vs mass data for the top tube and downtube.

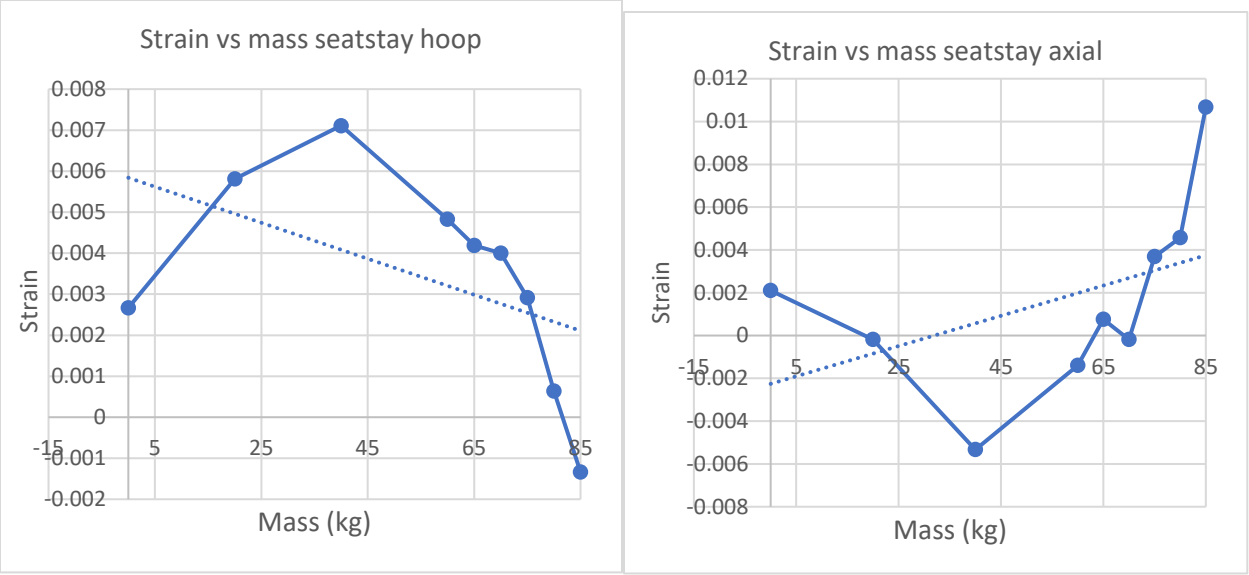

Figure 18: Plots of the strain vs mass data for the hoop seatstay strain gauge and axial seatstay strain gauge.

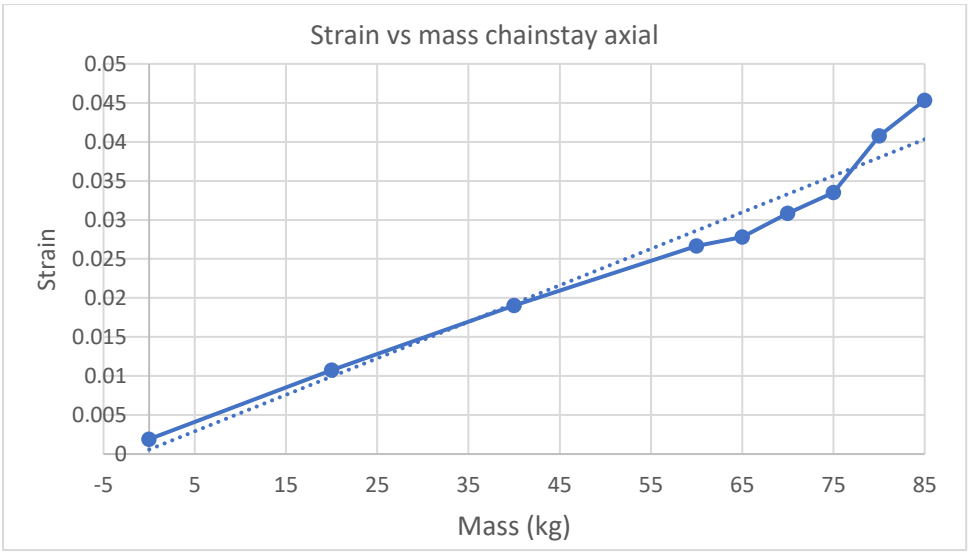

Figure 19: Plot of the strain vs mass data for the axial chainstay strain gauge.

3.4.2 Weighing.

This test was carried out by Kevin Palmer and the Mechanical Engineering Stores staff upon receiving the frame. The frame was weighed, and was shown to be 5.25 kg. This is significantly less than the weight range predicted in the PDS, and less than the value predicted by CAD, which was 6.103 kg. The values quoted in the PDS were maxima, rather than targets, and the CAD value was an estimate, so the test was carried out to check that the frame was below the

limit and in line with the value from CAD. Thus, the test was successful and the design criterion of the frame mass being in or below the 8-14 kg range for the frame has been met.
As an additional success, the mass of the frame as assembled for testing (including the steering assembly, saddle and seatpost, and wheels) was recorded and was found to be 10 kg.

3.5 Discussion of results.

The weighing of the frame yielded the results the group expected, in that the mass was less than that of the PDS weight range and only 0.85 kg less than the FEA predicted (6.103 kg vs 5.25 kg). This is most likely due to the densities of the materials in purchased components not exactly matching those used in CAD. This could be remedied by averaging multiple values for the density from many sources for a given material, but in this case the suppliers who were contacted to request data sheets did not provide them. As a result, it was decided to use values from the Solidworks library.

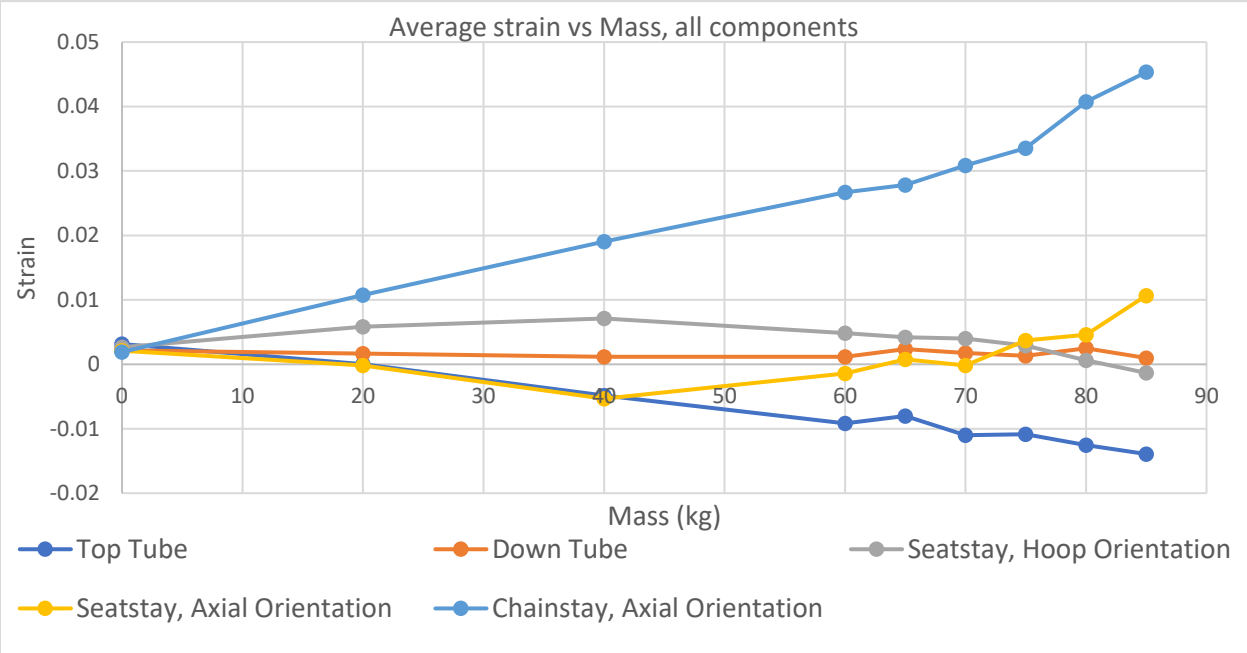

Figure 20: Plot of average strain against applied mass for all strain gauge locations.

The axial strain gauge at the chainstay join of the dropout exhibited higher values of strain over the loads applied, in line with expectations from the stress values attained in earlier FEA simulations. As can be seen in Figures Figure 12 (b), and Figure 13 (d) and (f), the highest value of stress occurs at the join where the chainstay meets the dropouts. Therefore, although the FEA did not predict significant differences in strains at the strain gauge sites (this could be refined as described in Section 3.6), the stress values being at their highest at this point indicates that the FEA was a realistic representation of this phenomenon, at least, and that the

predicted stress values are in fact higher at this join. The average data also follows a broadly linear profile, as predicted by the FEA strain values. That the data from the frame agrees well with the FEA in the case of trends, and that the frame itself did not exhibit damage during testing, means that the test can be described as successful. This is in the sense that, at the lower mass shown by the weight test, the frame was sufficiently strong up to and over the design load. However, there is some difference in the magnitude of the results displayed. The FEA predicts the trend of the results well in Figure 20 (in the case of the top tube, which was designated as a control area, and the chainstay), but the agreement is not exact due to the difference in magnitude of the data. The quality of the data is reasonable for some of the strain gauge sites, but in the case of the seatstay and downtube, the points themselves are fairly spread out and whilst a trendline can be fitted to them, they do not seem to follow as defined a trend as the chainstay or top tube. This could be due to a few factors. The main influence on the data is likely to be that the GTA who was assigned to apply the strain gauges did not have prior experience handling fitting strain gauges, as more experienced GTA was not available to advise on fitting, or fit, the strain gauges to the frame due to lack of personnel. One of the gauges was damaged during soldering, which reduced the data available for comparison. The seatstay gauges were also difficult to mount due to their position on the frame, which may have affected their performance as the process took longer than at other sites – e.g. the top tube. Furthermore, as mentioned previously, only two of the requested three readings were taken for some of the load values. When converted to stress, as in Table 7, the values calculated ranged from tens of MPa to the order of GPa, which was too high to correspond to what was observed in the test, since had the stress in the components been this high the frame would have failed (the value of approximately 9 GPa in the chainstay exceeds the UTS of the frame materials so failure would have been expected). Furthermore, this is significantly higher than the stress predicted by the FEA, which at 100 kg was 261.2 MPa (as in Figure 13 (f)), several orders of magnitude smaller than the data value, and the deformation being small implies that the FEA was the better representation of the frame's behaviour under loading than the strain data obtained from the gauges directly. This could also be due to the application of the strain gauges without more experienced personnel who normally would have been able to advise during the pre-test setup process. The large confidence intervals for some of the stress values cast some doubt on whether these are as good as they might have been had the difficulty with fitting the strain gauges not occurred. The strains at the seatstay were combined to find an absolute strain value calculated from a linear average from both the strain components. This was done to explore the overall trend in the strain at the seatstay join and see whether they could be usefully

combined to demonstrate a more cohesive trend. A shallow linear positive gradient resulted (visible in green in Figure 21), which became more tensile with increasing load.

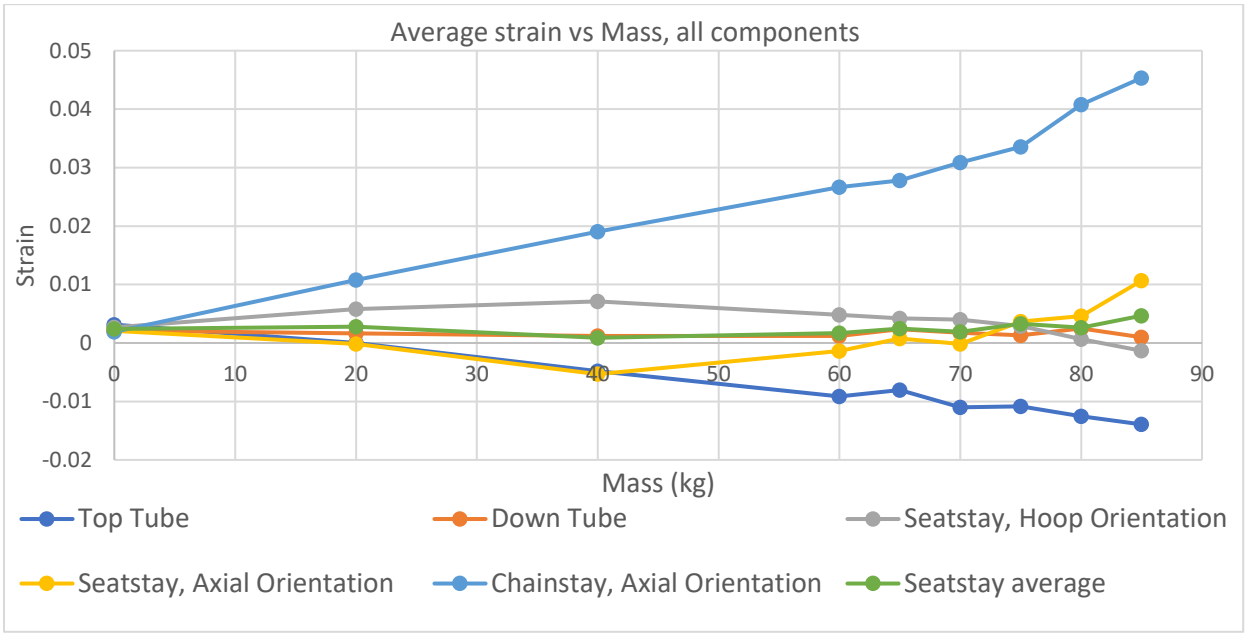

Figure 21: Average strain vs mass including the absolute strain in the seatstay.

This could be to do with a moment on the seatstay increasing as the load on the bike causes it to bow outward, like a simply supported beam sagging under loading. This same operation could not be completed for the chainstay since the hoop-oriented strain gauge applied to the chainstay was damaged during soldering. The sagging motion also drives the front fork down and outwards, which could explain the compressive stress on the downtube. This is because the join of the downtube and headtube is not at the base of the headtube, but is higher up, so the rotation of the headtube as the front fork rotates could be the cause of the compressive strain in the downtube, due to their relative angles. This sagging would also explain why the stress in the top tube is compressive, since if the frame were to sag, a compressive stress would be expected at the top. The principle, when applied here, explains the result well.

The positive chainstay strain indicates a tensile load, which is expected since the bottom bracket and seat tube are forced down by the applied mass, but the wheel supports itself.

The stresses are firstly obtained from the average strain measurements by directly multiplying the strains by Young's modulus ($\sigma = E * \epsilon$).

Table 7: Stresses within components according to average strain values (Units in kg and MPa).

Mass \ Component	0	20	40	60	65	70	75	80	85

Top tube	658.8	0	-1015.7	-1921.6	-1688.2	-2305.9	-2278.4	-2635.3	-2923.5
Downtube	452.9	350	247.1	247.1	494.1	370.6	274.5	521.6	205.9
Seatstay hoop	560	1220	1493.3	1013.3	880	840	613.3	133.3	-280
Seatstay axial	440	-40	-1120	-293.3	160	-40	773.3	960	2240
Chainstay axial	400	2260	4000	5600	5840	6480	7040	8560	9520

However, the data size is not large enough and has large fluctuations, then the 95% confidence intervals (CI) are obtained, by assuming the data are normally distributed, which is given by

$$(x_{lower}, x_{upper} = \bar{x} - z_{\alpha/2} * \frac{\sigma}{\sqrt{n}}, \overline{x} + z_{\alpha/2} * \frac{\sigma}{\sqrt{n}})$$

Where n is the size of sample i.e. the number of data obtained, $\bar{x}$ and σ are the mean and standard deviation of the sample respectively that both can be found using MATLAB. Corresponding to a 95% confidence limit, $z_{\alpha/2}$ is equal to 1.96. The CI indicates that for a component with certain mass, the actual value of stress is most likely (95%) in this range, and a reliable estimation of the true value could be made.

Table 8: The 95% CI for stresses (Units in kg and MPa)

Mass	Top tube	Downtube	Seatstay hoop	Seatstay axial	Chainstay axial
0	(-8341.6 , 9596.5)	(-5049.7 , 5912.5)	(533.3 , 533.3)	(-2001.2 , 2839.3)	(-4459.5 , 5221.4)
20	(-444,17 , 444.17)	(-25.13 , 691.80)	(980.1 , 1343.8)	(-401.80 , 325.61)	(1849.3 , 2455.5)
40	(-1457.6 , -477.0)	(235.29 , 235.29)	(875.9 , 1968.6)	(-1394.5 , 738.8)	(3431.0 , 4188.1)
60	(-1942.6 , -1717.6)	(-467.19 , 937.78)	(-488.8 , 1441.4)	(-1132.8 , 574.1)	(5144.1 , 5522.6)
65	(-8085.5 , 4869.8)	(-5508.8 , 6450.0)	(-130.0 , 1806.2)	(-1783.8 , 2088.6)	(-4593.8 , 6530.0)

70	(-5185.8 , 793.6)	(-2138.5 , 2844.4)	(316.0 , 1284.0)	(-522.14 , 445.9)	(6174.4 , 6174.4)
75	(-2619.9 , -1720.0)	(-36.18 , 559.05)	(365.58 , 802.67)	(260.2 , 1212.8)	(6515.5 , 6894.0)
80	(-2847.3 , -2172.3)	(-576.3 , 1569.8)	(-349.33 , 603.29)	(413.5 , 1415.0)	(7651.6 , 8653.1)
85	(-3282.6 , -2286.0)	(-2295.3, 2687.5)	(-3655.0, 3121.7)	(197.2, 4069.5)	(8099, 10035)

3.6 Implications of results.

The FEA method used for the predictions of the test results could have been refined prior to testing. The frame was modelled using a coarse mesh which was then improved and refined using mesh controls to capture the stress distribution in each component of the frame. Whilst some mesh refinement did occur and allowed the predictions to be made both on a component level and at the sites of the individual strain gauges, an additional step could have been taken. The sites of these stress concentrations could have been isolated, by modelling individual components or sections of components in the frame, for example, and a finer and more complex mesh could have then been used for even more accurate assessment of the stresses present in these areas.

The constraints used could also be reassessed in future simulations to be even more specific to each load case and to each component, however it was judged that since the frame would be supported in a stand during the load test and would be stationary, that fixing the location of the axles would appropriately represent the wheels supporting the frame in place.

The significance of the chainstay having higher strain than the other components, even though the strain and stress values seem rather higher than the FEA predicted, implying that the stress concentration is where it was expected to be in the frame, so begins to inform the focus for the redesign phase of the project.

The large confidence intervals in Table 8 also suggest that the data could have been more refined. This might have been achieved during testing with better strain gauge placement or more gauges, but also by allowing for a longer averaging period to eliminate the noise commonly introduced in the voltage values received by Madaq. Had the sampling rate of 1KS/s been used, the data might have had a smaller confidence interval which would have lent more credence to the results.

3.7 Summary of further testing.

Continuing from the test generation process in Section 3.1, dummy component tests were initially selected, intended to occur alongside manufacture of a full frame.

Test 1: Chainstay and Dropout Fatigue.

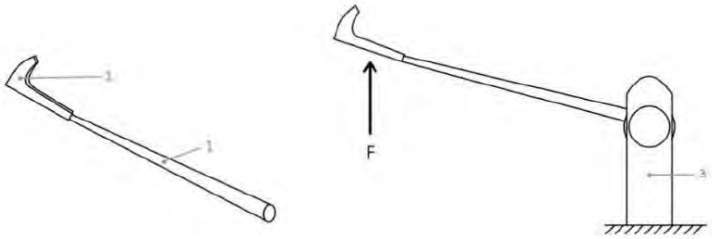

1	Chain stay
2	Drop out plate
3	Rigid Fixture

Figure 22: *Chainstay and dropout fatigue test. (Hales, Nag, Chabra, Cheng, & Huang, 2021)*

This subassembly was designed to test the resistance to fatigue in the rear section of the bike. Forces would be applied to a small section of the rear triangle at 1100 N and 10 Hz, over 100,000 cycles. This was close to the value quoted by the British Standard whilst being attainable with the facilities available to the group.

Test 2: Box Section Seat Tube Buckling.

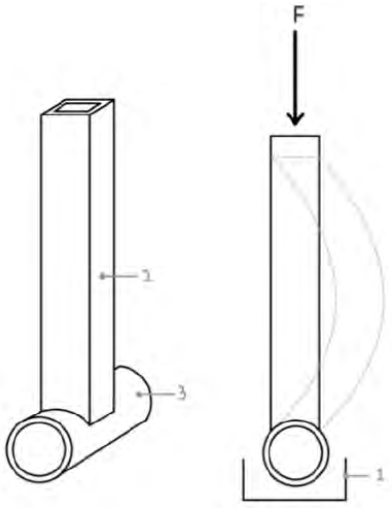

1	Instron Machine Clamp
2	Box Section Seat Tube
3	Bottom Bracket

Figure 23: Box section seat tube buckling test. (Hales, Nag, Chabra, Cheng, & Huang, 2021)

This subassembly was designed to test the axial strength of the seat tube, and the integrity of the join at the bottom bracket. A 1000 N force would be applied, which was greater than the weight force of the 80 kg rider, to ensure the component was sufficiently strong. The analysis did not predict significant strain in this component, but it was deemed useful to test its performance outside of the design values of the frame.

Test 3: Bottom Bracket Brazed Joint Fatigue.

This test, using a similar subassembly to the previous, was designed to test the strength of the brazed joint at the bottom bracket when pedalling forces were exerted on the frame. As with the first test, a 1100 N force would be applied at 10 Hz for 100,000 cycles.

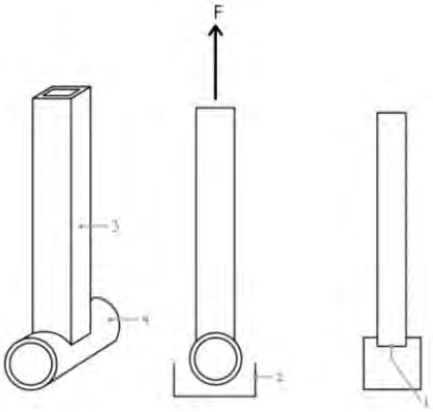

1	Brazed Joint
2	Instron Machine Clamp
3	Box Section Seat Tube
4	Bottom Bracket

Figure 24: *Bottom bracket joint fatigue test. (Hales, Nag, Chabra, Cheng, & Huang, 2021)*

Test 4: Top Tube Impact Fracture.

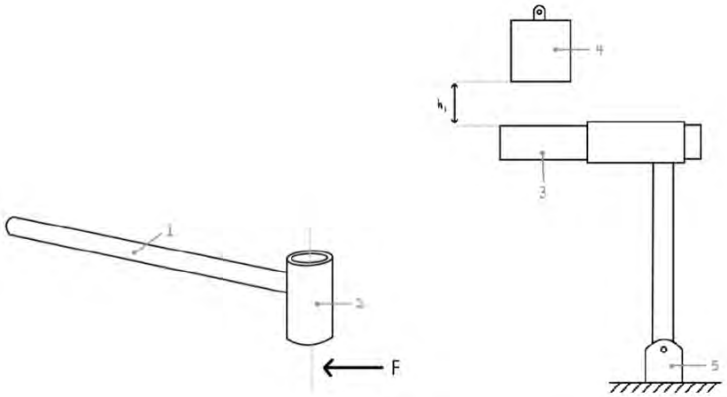

1	Top Tube
2	Head Tube
3	Circular Impact Bar
4	Striker Mass (22.5 kg)
5	Rigid Fixture

Figure 25: *The top tube impact fracture test. (Hales, Nag, Chabra, Cheng, & Huang, 2021)*

This test was intended to verify that the frame could withstand a head-on impact (for example, a collision). The top tube was expected to be most significantly affected, and the test was designed with a 22.5 kg striker dropped from 360 mm (=h1), as per the British Standard.

Test 5: Down Tube Brazed Joint Pedalling Fatigue.

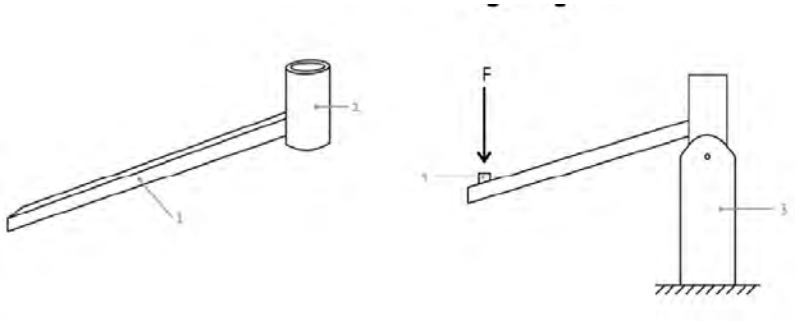

1	Down Tube
2	Head Tube
3	Rigid Fixture
4	Flat Knob

Figure 26: *Down tube joint pedalling fatigue test. (Hales, Nag, Chabra, Cheng, & Huang, 2021)*

This test was designed to test the strength of the join at the bottom of the head tube, as pedalling forces would be transferred through the downtube during riding. These forces would exert a force on the joint between the down tube and the head tube. The force applied was the same assumption for pedalling forces, 1100 N at 10 Hz over 100,000 cycles.

The second dummy component testing method planned to make a dummy rear triangle of the bike frame. This would be beneficial as it not only saves set-up time for technicians, but also lowers the cost for the dummy component. The rig proposed in Figure 27 below is the 100T ESH HR, a 100-ton capacity high-rate test machine. However, this method was later proven to be unfeasible as the rear triangle on its own is too big to fit in any testing rigs in the department.

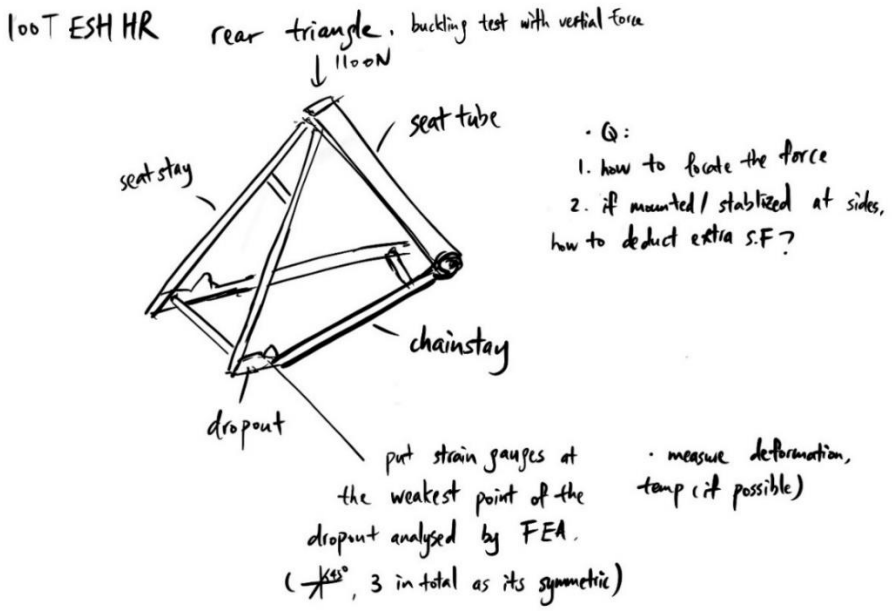

Figure 27: A sketch of the test setup for the rear triangle test.

As mentioned in Section 3.1, conducting dynamic tests was impractical due to limitations on time and testing resources. Therefore, the remaining tests were the box section seat tube buckling and top tube impact fracture. In addition, the department did not approve extra funding for dummy components.

As discussed in Section 3.1, multiple tests were planned over the course of the project. Some of these were curtailed by not having access to industry-standard machinery, for example, the equipment used to test production bikes in large quantities (specified by the British Standards to which the PDS aimed to test the bike). Some of the tests had to be removed as they would be too costly to undertake. Manufacturing only the individual subassemblies would have deprived other groups of a proper platform on which to showcase their work (since, although not planned for testing purposes, it is hoped that the full frame with all its components can be assembled

towards the end of DMT). In addition to this, one of the desired tests was an impact test, but despite repeated attempts, the group was unable to gain access to a drop tower since, as in Section 3.1, the personnel able to access these facilities were restricted. All of these factors led to the decision to build and test the full frame as originally intended.

The key outcomes from the tests which were performed were that the frame succeeded during the weight test as its mass was below the design values, and in addition to this the frame performed well in the non-destructive static load test, showing little deformation, and not experiencing damage or failure, even at a load greater than the design weight. The fact that this was achieved despite being below the target mass is encouraging. The fact that the FEA results match the trends of the test data lend confidence to both data sets, since the predictive simulations behaved as expected even though the magnitude of the values was smaller than those returned by the test. These points validate the design as specified by the group, but the stress concentration around the dropout interface has been flagged as a concern for a while. The increased strain at this point (the chainstay interface specifically) shows this is clearly still an area worth considering and could be strengthened further to provide additional security.

3.8 Detailed redesign.

No components showed signs failure or damage after non-destructive testing. However, pre-test finite element analysis had repeatedly highlighted a particular area of abnormally high stresses, the dropout-seat stay interface. In fact, the stresses in this region meant that the minimum safety factor of the frame, based on the von Mises failure criterion, was found to be 1.1. This is lower than the target value stated in the initial design specification. Figure 28 shows the von Mises stress plot at the dropout interface. The stresses in this region are approximately three orders of magnitude higher than the rest of the frame, as shown in Figure 13 (f).

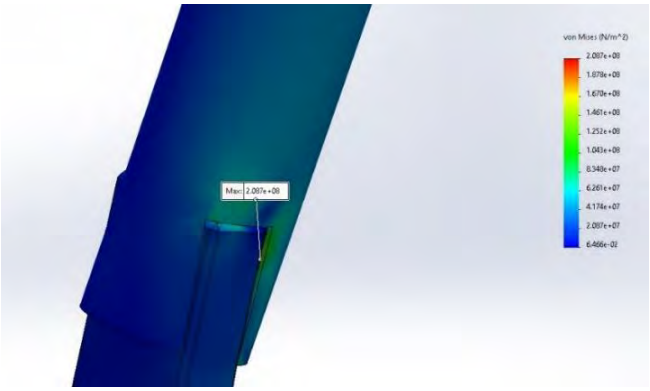

Figure 28: von Mises stress plot at the dropout-seat stay interface for nominal loading conditions. (Hales, Nag, Chabra, Cheng, & Huang, 2021)

While the stresses in thin dropout backplate itself remain relatively low, the sharp corners of cut-outs are major stress raisers in the frame and are main sources of concern. Furthermore, the plated dropout design features eight similar stress raisers. Another issue with the manufactured dropout design were its low weldability and brazeability. This stemmed from the limited contact-surface-area between the backplate and the respective joining tubes. Due to the complex geometry the weld paths were also abrupt. Not only did this make the component hard to join, but the bonding strength was also compromised. This problem was not easy to overlook due to the lack of dynamic load testing needed for reliability. It is often observed that weld joints are the first areas to fail under fatigue loading conditions (Meneghetti & Campagnolo, 2018).

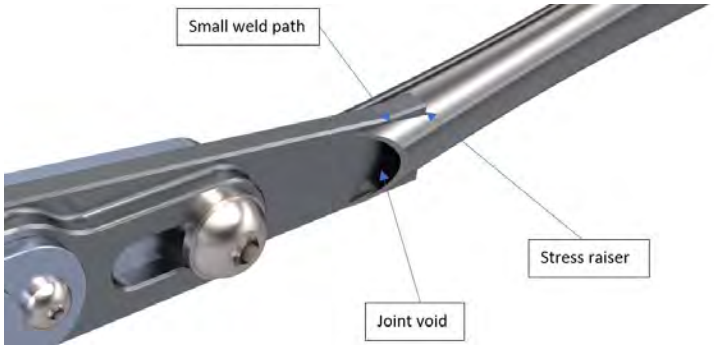

Figure 29: Problems with current dropouts interface design.

The dropouts were the most carefully designed component of the frame, having gone through several dedicated iterations. However, it was due to the combination of the discussed problems that a redesign focused on this component was of importance. These problems directed the new design. First, the interface must be clear of obvious stress raisers. Second, the new design must have a larger contact surface area both easier welding and for a stronger joint.

Figure 30: Current full rear dropout assembly.

The current sliding dropout assembly as shown in Figure 30, allowed for easy tensioning of the chain while keep the brake callipers aligned with the disc rotors on the wheel hub. The design

featured a two-piece steel backplate and two CNC-machined aluminium dropout inserts for each side. The two-piece steel backplates were individually laser cut, then welded together to achieve the stepped design. This technique was developed instead of CNC to minimize manufacturing costs while conforming to the original footprint. The inserts on the other hand remained a complex part, requiring threading and bi-directional planar cuts. This increased the overall CNC cost. Together with the several stages of manufacturing for the backplates and the complex inserts fabrication, the overall assembly turned out to be the most expensive and time-consuming sub-assembly of the frame. The complexity of the current design is demonstrated in Figure 31 detailing the components in the left dropout sub assembly.

Figure 31: Exploded view of components part of current left side dropout subassembly.

For the revised design, the concept of sliding dropouts was conserved, still providing 16cm of tensioning adjustability but improves on the numerous problems of the current design. The redesign, as shown in Figure 32, was also seen as an opportunity to design a cheaper alternative. While at first glance, the design seems to maintain its complexity, it can be observed that the fabrication difficulties of the previous design are generally negated. Firstly, the backplate only requires one-time orientation in the CNC machine as all necessary cuts can be achieved by a vertical router drill bit on a solid steel block. This is achieved by considering a different disc brake standard, the ISO mount, instead of the Flat mount standard as deployed in the old design. ISO standard disc brake mounts can easily be fitted via an after-market adapter to accommodate for a native flat-mount calliper. Thus, any calculations and dimensions made for the previous brake callipers could be directly translated on to this design.

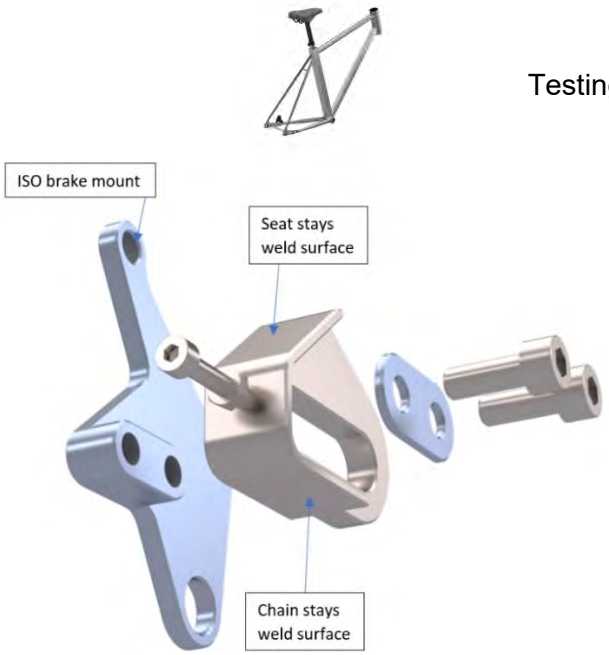

Figure 32: Exploded view of components of redesigned left side dropout subassembly.

Overall, the volumetric footprint of the main plate raw material has almost been halved, as shown in Figure 33. A detailed analysis of the two pre-machined bodies can be seen in Figure 44 and Figure 45 (in Appendix 7.3). A mass properties evaluation on SolidWorks between the two machined main plates revealed a 42% weight reduction, as shown in Figures Figure 46 and Figure 47 (also in Appendix 7.3). Being the only solid body component of the frame, compared to hollow tubes, weight reduction in this area vastly improves riding conditions by transferring fewer dynamic loads from the rear wheel. A more subtle benefit of this is the saved material cost and standardisation of fasteners. For a one-off project such as this, custom dropouts are usually not offered by bicycle manufacturers, thus materials are not stocked in-house and require out-sourcing. This means that any additional material increases the cost, as experienced with the current design.

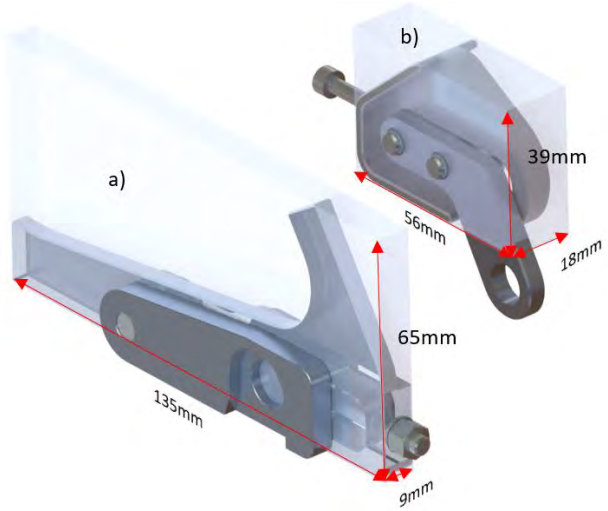

Figure 33: Cartesian footprint of the respective main plates in the right-side assemblies of a) the current design and, b) the redesigned. Both axle holes are aligned to show relative positioning.

More significantly, the hooded design tackles the problem of weldability. Instead of having plates that engrave into the tubes, the hoods provide a flat surface for the circular tubes to sit against. This surface interface is like the other tube interfaces in the frame allowing for a large, uniform weld bead path along the circular contact edge. As a result, mitigation of the use of additional weld caps as no joint voids are created, as seen in the plated design. The new hooded dropout backplate also has more forgiving curved edges and essentially eliminates any present stress raisers. A small feature included in the redesign is the improved tensioner screw placement. By placing the bolt inside the rear triangle instead of protruding out of it, it reduces the lateral length of the bike. Furthermore, it also protects the threads from a direct spray of grit from the wheels.

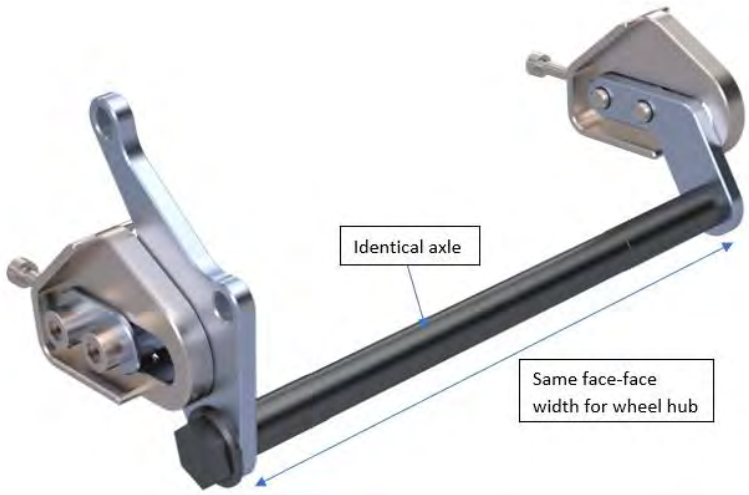

Figure 34: Redesigned dropouts full rear assembly using the same axle from current design.

To minimize any additional costs that could arise from implementing the redesign, any dropout dependant dimensions of other components, such as the rear axle, are kept the same. Figure 34 shows the updated rear assembly featuring the same dependency dimensions. This means that to retrofit the redesign, most of the existing frame can remain and only the rear can be altered. The only additional costs would be the material and fabrication of the new dropout plates. Like the previous design, a way to reduce the required budget even further would be to weld the flanged hood separately. However, this technique has specifically been avoided to reap the benefits of having an unibody part, reduced fabrication time, and greater strength.

As a final note, along with considerations expressed about the stress raisers present within this assembly, the group recognises that the frame itself could be made lighter through tube section or diameter changes, or material alterations – however, since the budget for this redesign was stipulated to be the original amount of £1000 for all DMT groups, the frame would have been too expensive to machine again as a whole, as the first iteration incurred total manufacturing costs of in excess of £1200 for the bespoke frame. The dropouts in the first iteration came in total to

roughly £800, putting them within the redesign budget, and therefore to ensure the group remains within the constraint as advised by the department for this section of the project, the dropouts are the only area available for consideration.

4 Discussion

4.1 Review of design.

The final design with all sub-assemblies fitted is rendered in Figure 35. The frame subassembly was the result of numerous design iterations. Each iteration tackled intrinsic flaws, problems identified from within the sub team, and extrinsic issues imposed by other sub-groups. However, the continuous development of the design is reflected in the final product, one that has deviated significantly from the initial concept yet still safely meets the design criteria. This section aims to critique the final design while also analysing specific parts and how successful their respective roles are when compared to the design specification and existing products on the market.

Figure 35: The final CAD model of the bicycle frame with all components present.

4.1.1 Construction.

As discussed in Section 3, the frame met the weight and static load bearing specifications. However, it is important to recognise these specifications as being self-selected and having manufacturing difficulty considerations for a one-off product. Standard (non-electric) bicycle frames available in the market utilise pre-manufactured specialised bicycle tubing. Modern tubing is usually made from aluminium alloys, or the frame is fabricated as a single carbon fibre shell. These techniques mean that modern standard frames are generally around 2 kilograms

compared to approximately 5 for this one. While such a comparison could easily deem the final designed frame as a failure when discussing the construction, it must be noted that standard bicycles are exposed to lower loads than e-bikes. The weight is much more comparable to current market e-bikes. The design features a combination of bicycle-specific Columbus steel tubing and custom mild steel tubes, necessary to accommodate the niche requirements of the frame such as having flat surfaces for the seat tube and downtube to weld on the motor plate and provide a mounting point for the battery. The oversized headtube was also a custom part, having to accommodate ISO standard bearings of the steering assembly instead of conventional smaller bicycle bearings. Lastly, the multi-component dropouts were made from stainless steel and aluminium alloy inserts, as discussed in Section 3.8.

Use of custom-made parts such as the ones discussed above, and the impact of the pandemic on the manufacture process and access to College facilities, meant that budgeting had to also include machining costs, thus lower grade materials were chosen. Furthermore, bespoke components had to consider possible manufacturing defects and thus dimensions like wall thickness were chosen to be more conservative. This was advantageous for the brazing process as components generally held their respective shapes well (the exception being the head tube, which is discussed in Section 2.1).

The biggest challenge for designing bespoke components required materials to be in stock and fabrication methods available in the contracted workshops. This solidified the case for using a more workable material such as steel rather than a lighter material such as aluminium which is harder to machine. This also allowed for a greater range of potential joining methods such as TIG welding and brazing, increasing the flexibility in choice for a joining method whilst keeping the frame sufficiently strong.

Figure 36: CAD render of the isolated frame assembly.

The above conditions such as thicker components constrained the frame from reaching an “optimal” weight. However, given the circumstances, achieving the properties that the frame

demonstrated during testing (whilst still weighing less than expected) is seen as a success. The final design for the frame is shown in Figure 36. There are clear areas in which this design could be improved. Section 3.8 highlights the most critical area to redesign, given the £1000 budget assigned for the second iteration. However, if financial limitations were relaxed and there was access to a greater range of workshops with more advanced engineering tools, more advanced frame designs as explored in previous design iterations could be implemented. This is further explored in Section 4.2.

4.1.2 Anthropometrics and usability.

The frame geometry and riding position of the user play a big role in how the bicycle handles and feels. This was recognised early on, however anthropometric oriented design proved to be difficult. Changing any specific component dimension would have a direct impact on the dimensions of other parts. For example, fixing the length in between the saddle and bottom bracket to ensure a comfortable pedalling position also changed the horizontal length in between the saddle and handlebar. This elongation would stretch the rider out leading to an uncomfortable and aggressive riding position, not suitable for urban commuting. Furthermore, the wheelbase would be altered, causing an unbalanced weight distribution.

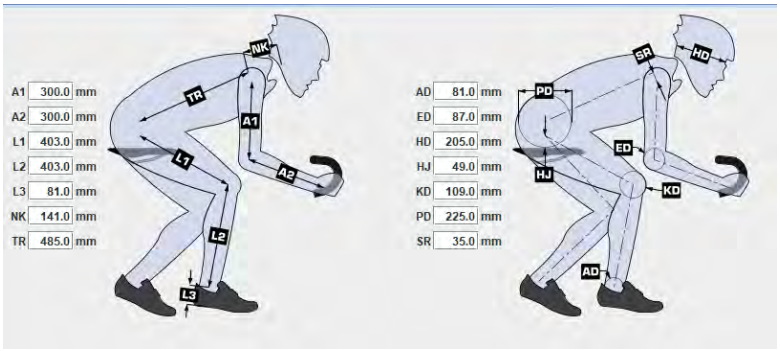

Figure 37: Inputting user dimensions for geometry calculation using BikeCAD.

To reduce the guesswork required for achieving a geometry to suit a comfortable riding position while maintaining its structural integrity, a specialised software called BikeCAD was used, as shown in Figure 37. The frame was designed for users of average height, around the region of 5 ft. 8 in. – 6 ft. 8 in. tall. The use of an industry-standard software as a guide ensured the proposed dimensions suited the required ride conditions. This allowed the team to check the effects of altering any materials or specific dimensions to meet structural requirements.

4.1.3 Subgroup integration.

At a glance, the e-bike design differs significantly from conventional bicycle design. Firstly, the chosen method for integrating the motor and gearbox assembly was by using a motor backplate. This design was chosen for its ease of welding on to the square profile seat tube of the frame, only requiring long linear weld paths. The simplicity of this method helped with fabrication costs. It also allowed for the main frame to be manufactured separately from the motor plate, made externally. However, the 5 mm thick plate had to be welded to one side of the seat tube. This adds significant off-centred weight to the frame. Having motor loads being transmitted through an unbalanced mass will likely lead to an unnatural riding feel. Another potential problem with this design is the placement of the protruding drive sprockets. These rotating protrusions are close to the rider's right knee and is a cause of concern without some form of motor casing.

Similarly, the battery pack also called for a square-sectioned tube to be mounted onto. However, a bolted method of integration was opted for this adding the ability to remove the battery if required. The lack of space to fit the motor can be seen Figure 35. Even with a side slotting design, this is certainly an area that could be redesigned for better manufacturability and usability. The tight fit forces extremely precise tolerances for the placement of the downtube holes, shown in Figure 36. To cater for the side-sliding fit, an additional bracket that sat on the frame had to be manufactured. However, these brackets relied on having thru holes in the downtube. While this did not end up causing any problems, any warping of the downtube during brazing, or misplaced holes, could have caused the battery to be unmountable.

Lastly, the steering headset assembly was attached via a through headtube, part of the frame. Once again, the simplicity of the design (it has no internal steps) made manufacturing of the part easy. Finding the raw materials needed for the custom part was also relatively straightforward. Unfortunately, due to a miscommunication and late design change, the headtube wall thickness had been quoted for an internal diameter smaller than that which was required. Owing to the simplicity of the design, this last-minute change of the internal diameter was possible but required further machining, delaying shipping by a week and increasing costs. Additionally, the now thinner head tube was vulnerable to thermal deformation. In the future, designing to the correct diameter would simply require a thicker wall. More critically, the overall frame design assumed front forks and crown to be of the same relative density as the rest of the frame. Unfortunately, the final design featured a solid forks and crowns. This shifts the centre of gravity towards the front of the bike. Dynamic loads transmitted through the front wheel will also be more pronounced.

4.2 Overview of future design progression.

After the manufacture of the frame was complete, and during assembly, the STW raised the issue that the head tube had become warped, as discussed in Section 2. This could have been due to multiple factors. The head tube was not a standard size for a bicycle, and it was influenced by the design of the headset assembly to ensure that this could be accommodated properly. In future iterations, and after discussion with subgroups, the headset diameter might be altered or reduced to a standard size such that this can easily be changed if needed (and standard bicycle headset bearings can be used). Additionally, the effect of the diameter of the head tube could have caused the material to warp during joining, so reducing this could eliminate the deformation during the building of the frame. The material used was mild steel, which in hindsight could be replaced with a carbon steel for increased strength and heat resistance during joining. This would also serve to reduce the likelihood of deformation.
Some other potential design refinements include leaving more space for the battery and motor by altering tube sizes, as well as cable routing either internally or externally using eyelets or drilling through tubes to contain and protect it. Additionally, the hole for the through axle could have been made smaller as this might have made threading easier for the manufacturer. This would have removed a step for the STW in the assembly process. The brakes being loose on the axles should be amended in the future with either a new wheel or a better axle or hub support. Although the frame did turn out to be lighter than the PDS and CAD weight, further weight decreases would be beneficial. However, to maintain the same performance with lower weight, more advanced materials will need to be used. This can be a costly endeavour, but a potential consideration should there be a larger budget in the future. Once testing has been completed, both current and future (to validate the design for commercial use), the frame might be painted to improve its aesthetics. Finally, better design integration between different sub-assemblies could result in better placement of the other components within the frame, as the tolerances for these were very tight. For example, the motor plate could have been integrated into the frame structure in such a way that more space would have been left for the battery, even though this ended up being outside the originally stated envelope.

4.3 Review of how the group progressed the project.

The approach to project management started off very strong. Roles were defined and a Gantt chart was built. However, sticking to the initial plan was where the group went awry. While some roles were well defined and performed in a timely fashion, there were several tasks that did not clearly fall under any one group member’s responsibilities. There was hence some confusion as

to which member should take on these ad-hoc roles. Hence, in hindsight, better allocation of ad-hoc tasks would have been ideal. While there were not many delays in completing these tasks, some of the group members were overloaded. Additionally, communication amongst the group was hindered by time zone differences and logistical issues. It was difficult getting all members on a call together to regularly check progress on the project. The only meetings at which the group was regularly able to have all members present were with the supervisor, which helped bring members up to speed, but was insufficient in allowing the group to work together as a team, since these meetings only occurred once weekly. The lack of communication caused some overlap in work and led to a disjointed design report, which then took quite some time to fix near the deadline. Fortunately, the group took this as a learning experience and worked more synchronously for the remaining deliverables. Additionally, some members were exceptionally good at their tasks, such as design and advanced analysis using engineering software, which elevated the overall quality of the project. It was beneficial having members with prior engineering related work experience, which brought an additional level of complexity and professionalism to the project.

The cost of materials and manufacturing was grossly underestimated at the beginning of the project. The initial £1000 budget was quickly exceeded. Several design iterations had to be made to simplify manufacturing and keep costs low. The budgeting foresight that comes from experience was lacking in the team. However, the supervisors were able to pre-empt some potentially costly design decisions made by the team. Eventually, a budget extension had to be requested. It is likely that this could have been avoided, had the cost been kept in mind from the very beginning. The costs that were unexpectedly high mainly came from manufacturing. Producing single, bespoke pieces was naturally expensive, so tubular components were kept as close to standard dimensions (as provided by suppliers) as possible.

While internal deadlines were still being met, a lot of the delays in the project came from miscommunications or delivery mishaps from suppliers. The delivery of the frame was missed several times, which delayed testing. Despite this, the group was still able to obtain test results on time. In hindsight, a greater cushion for delays while dealing with external parties could have been planned.

Finally, due to the remote nature of the project, access to important software was limited. For example, some members were not able to access FEA and CAD software due to connectivity issues and the lack of access to college computers. This limited the number of people who could contribute to those tasks and slowed down work.

5 Conclusions

FEA predictions were dependent on the material properties used but predicted stress and strain values were lower than those achieved by the data. In the sense of trends and general predictions, of relative magnitudes, the data conformed well to the expected pattern of results and thus demonstrated that the FEA was a valid model for the tests performed. This is notwithstanding the discrepancy between the size of the strain in the FEA and in the results (as described in Sections 3.3, 3.4, and 3.5). This could have been influenced by a combination of the experience of the personnel setting up the test and the properties and refinement of the finite element model, as well as the load case used in the simulation. Overall, the FEA was judged to be a good prediction of the behaviour trends of the frame, even if the magnitudes of the data collected during testing did not match this. Despite this discrepancy, the simulation predicted that the frame would perform well in the static load test, and the capacity of the frame to support loads up to 85 kg with no noticeable damage reflects this.

While the final product was quite different in terms of design and performance to what the group had initially planned for, it can still be deemed a successful project. Given the tight budget, being able to come below the target weight without using ultralight materials like carbon fibre was a significant accomplishment. In the initial research that was conducted, a major consumer concern for e-bike performance was the range. Being able to keep the weight low was therefore a contributor for the type of performance users seek. In terms of static performance, we deem the tests to have been satisfactory. Being able to minimally withstand the weight of the rider classifies the product as a functional, a success given the harsh conditions under which the project was conducted. However, while the tests were successful, the bicycle is not yet ready for commercial use. The project was a fantastic first iteration of the e-bike, but will greatly benefit from further, more rigorous performance testing in the future. User safety in such a product should be top priority. Hence, high impact and long duration dynamic tests must be conducted before the e-bike can be commissioned for use. Nevertheless, the needs of the project were not as stringent as we set them out to be. In the context of a university engineering project, the group was successfully able to manufacture a functional, robust, cost and weight efficient frame.

6 References

BSI, (2017). BS EN 15194:2017 *Cycles – Electrically power-assisted cycles - EPAC bicycles*, *BSI Standards Publication.* Available from : https://bsol-bsigroup-com.iclibezp1.cc.ic.ac.uk/Bibliographic/BibliographicInfoData/000000000030384746

Hales, Nag, Chabra, Cheng, & Huang. (2021) Design Report DMT Group 1A.

Mark Bowkett & Kary Thanapalan (2017) Comparative analysis of failure detection methods of composites materials' systems, *Systems Science & Control Engineering*, 5:1, 168-177, DOI: 10.1080/21642583.2017.1311240

Strain Gauges and Wheatstone Bridge Measurements.pdf. Blackboard.com, adapted from Measuring Strain with Strain Gauges. *National Instruments Application Note (1998)*. p78.

Vanwalleghem, J., De Baere, I., Loccufier, M. & Van Paepegem, W. (2018) Development of a test rig and a testing procedure for bicycle frame stiffness measurements. *Sports Engineering*. [Online] 21 (2), 75–84. Available from: doi:10.1007/s12283-017-0248-8.

Meneghetti, G., Campagnolo, A. (2018) The Peak Stress Method to assess the fatigue strength of welded joints using linear elastic finite element analyses. *Procedia Engineering*. Volume 213, p 392-402. Available from https://doi.org/10.1016/j.proeng.2018.02.039.

7 Appendices

7.1 FEA Data.

Table 9: Top tube strain vs mass.

Mass (kg)	Max	Min	Avg	RMS
0	2.82E-06	1.39E-08	6.1E-07	6.85E-07
20	6.02E-06	5.26E-08	1.51E-06	1.67E-06
40	9.24E-06	5E-08	2.43E-06	2.72E-06
60	1.25E-05	8.31E-08	3.36E-06	3.78E-06
65	1.33E-05	6.55E-08	3.59E-06	4.05E-06
70	1.41E-05	7.91E-08	3.83E-06	4.31E-06
75	1.49E-05	8.78E-08	4.06E-06	4.58E-06
80	1.57E-05	5.35E-08	4.29E-06	4.85E-06
85	1.65E-05	3.7E-08	4.53E-06	5.11E-06
90	1.73E-05	5.69E-08	4.76E-06	5.38E-06
95	1.81E-05	8.83E-08	4.99E-06	5.65E-06
100	1.89E-05	7.87E-08	5.22E-06	5.92E-06

Table 10: Left chainstay strain vs mass.

Mass (kg)	Max	Min	Avg	RMS
0	5.75E-06	4.78E-08	1.3E-06	1.37E-06
20	3.04E-05	2.29E-07	7.98E-06	8.29E-06
40	5.51E-05	4.59E-07	1.47E-05	1.52E-05
60	7.98E-05	6.91E-07	2.13E-05	2.21E-05

65	8.6E-05	7.49E-07	2.3E-05	2.39E-05
70	9.21E-05	8.07E-07	2.47E-05	2.56E-05
75	9.83E-05	8.65E-07	2.63E-05	2.73E-05
80	0.000105	9.23E-07	2.8E-05	2.91E-05
85	0.000111	9.81E-07	2.97E-05	3.08E-05
90	0.000117	1.04E-06	3.13E-05	3.25E-05
95	0.000123	1.1E-06	3.3E-05	3.43E-05
100	0.000129	1.16E-06	3.47E-05	3.6E-05

Table 11: Right seatstay strain vs mass.

Mass (kg)	Max	Min	Avg	RMS
0	1.71E-05	1.54E-07	1.46E-06	1.58E-06
20	8.77E-05	7.81E-07	9.04E-06	9.42E-06
40	1.58E-04	1.41E-06	1.66E-05	1.73E-05
60	0.000229	2.04E-06	2.42E-05	2.52E-05
65	0.000246	2.2E-06	2.61E-05	2.71E-05
70	0.000264	2.35E-06	2.8E-05	2.91E-05
75	0.000282	2.51E-06	2.99E-05	3.11E-05
80	0.000299	2.67E-06	3.18E-05	3.3E-05
85	0.000317	2.82E-06	3.37E-05	3.5E-05
90	0.000335	2.98E-06	3.56E-05	3.7E-05
95	0.000352	3.14E-06	3.75E-05	0.000039
100	0.00037	3.29E-06	3.94E-05	4.09E-05

Table 12: Strain vs mass for down tube.

Mass (kg)	Max	Min	Avg	RMS
0	1.22E-05	1.16E-08	7.89E-07	9.17E-07
20	4.37E-05	8.8E-07	3.53E-06	3.75E-06
40	7.52E-05	1.51E-06	6.27E-06	6.63E-06
60	0.000107	2.14E-06	9.02E-06	9.51E-06
65	0.000115	2.3E-06	9.7E-06	1.02E-05
70	0.000123	2.46E-06	1.04E-05	1.09E-05
75	0.00013	2.62E-06	1.11E-05	1.17E-05
80	1.38E-04	2.78E-06	1.18E-05	1.24E-05
85	1.46E-04	2.93E-06	1.24E-05	1.31E-05
90	1.54E-04	3.09E-06	1.31E-05	1.38E-05
95	0.000162	3.25E-06	1.38E-05	1.45E-05
100	0.00017	3.41E-06	1.45E-05	1.53E-05

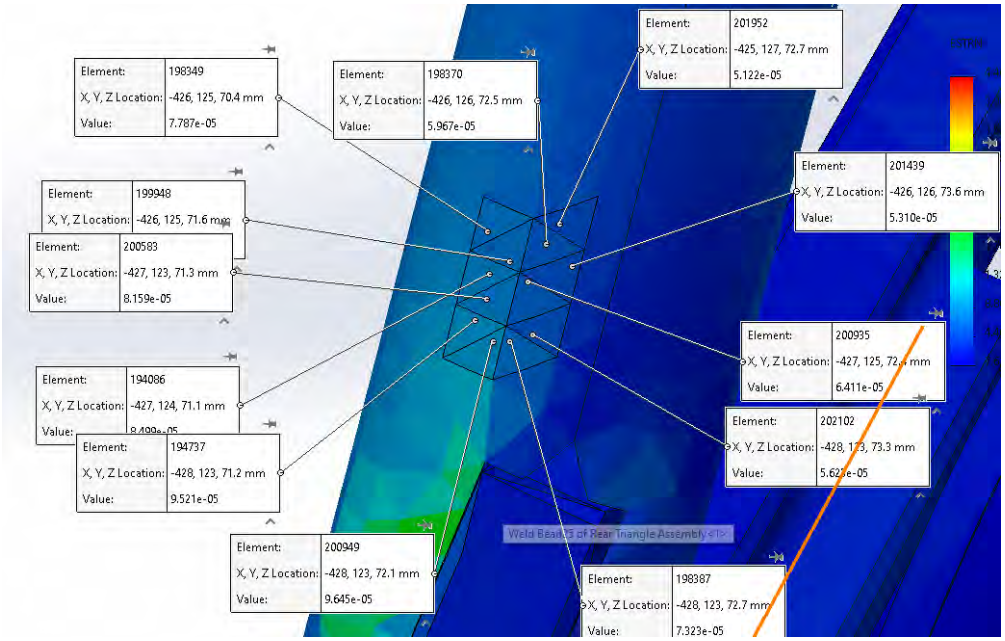

Figure 38: Finite elements at axial strain gauge site on right seatstay.

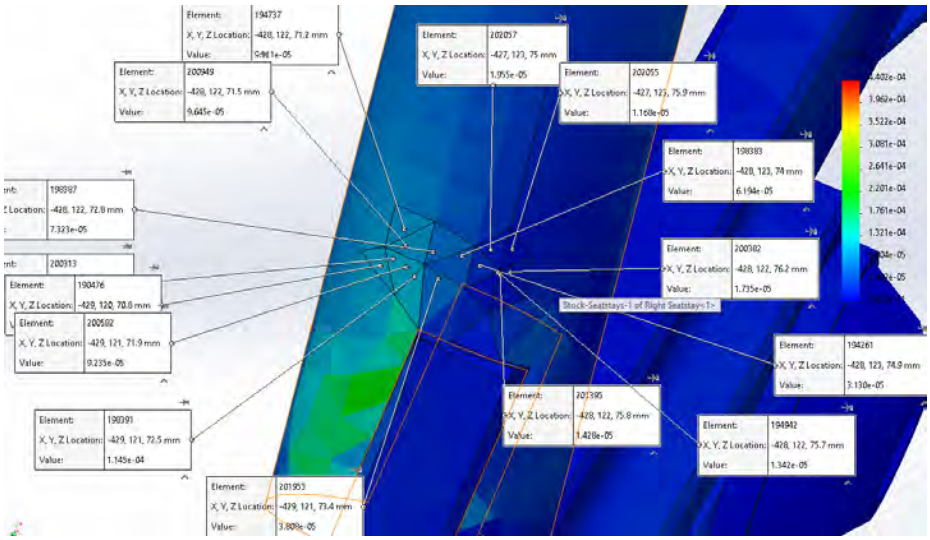

Figure 39: Finite elements at hoop strain gauge site on right seatstay.

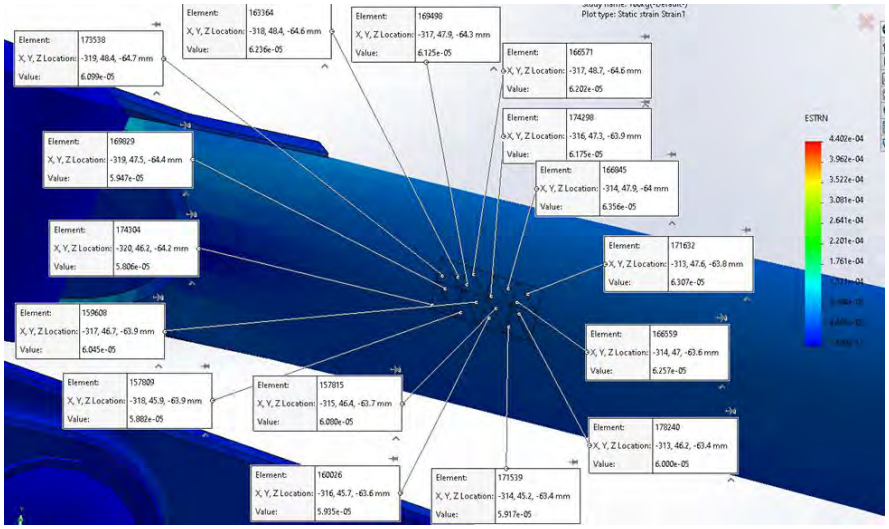

Figure 40: Finite elements at axial strain gauge site on left chainstay.

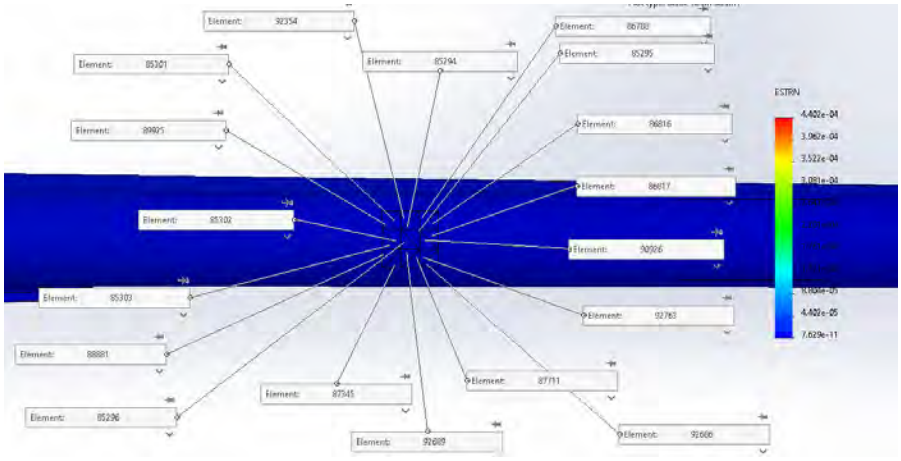

Figure 41: Finite elements at strain gauge site on top tube.

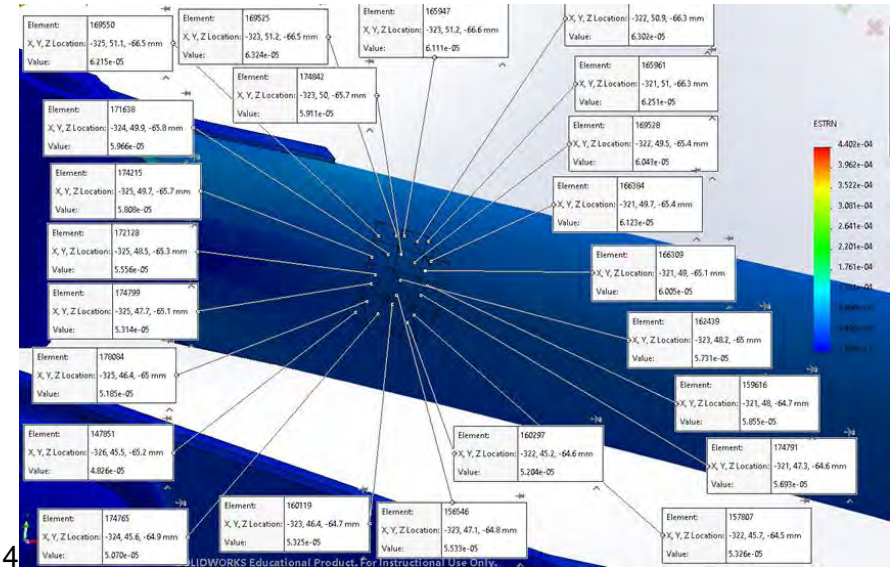

4

Figure 42: Finite elements at hoop strain gauge site on left chainstay.

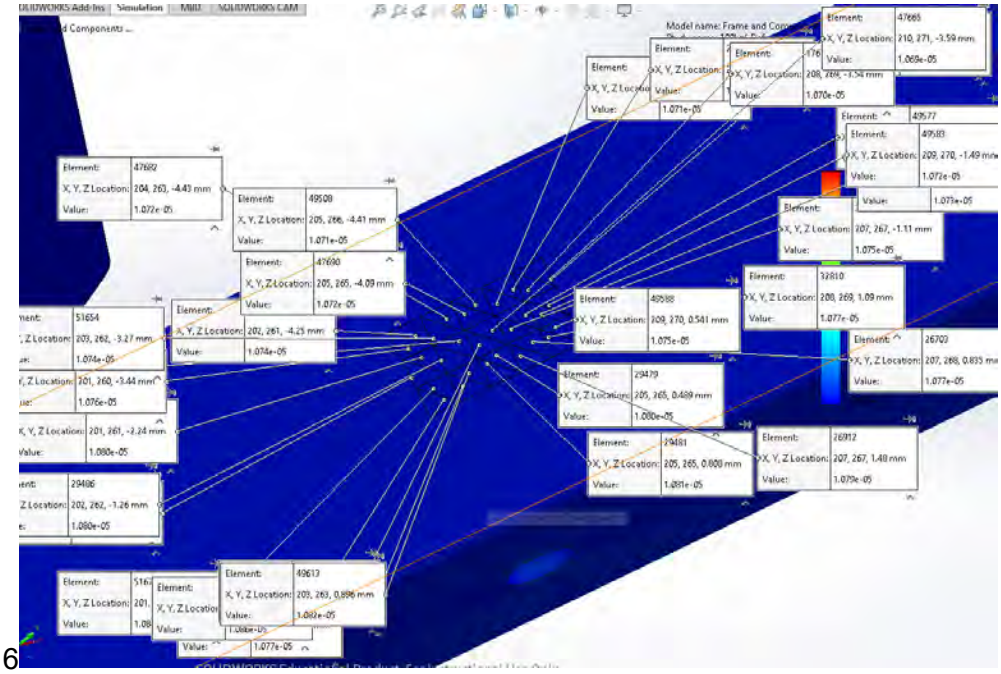

6

Figure 43: Finite elements at strain gauge site on down tube.

7.2 Test Data.

Table 13: Raw voltage and mass data from the test.

Mass (kg)	Channel	Component	Voltage 1(V)	Voltage 2 (V)	Voltage 3 (V)	Voltage 4 (V)	Avg. Voltage (V)
0	1	Top tube	0.017	-0.001			0.008
0	2	Downtube	0.011	0			0.0055
0	3	Seatstay hoop	0.007	0.007			0.007
0	4	Seatstay axial	0.008	0.003			0.0055
0	5	Chainstay axial	0	0.01			0.005
20	1	Top tube	-0.002	0.003	-0.004	0.003	0
20	2	Downtube	0.005	0.006	0	0.006	0.00425
20	3	Seatstay hoop	0.016	0.014	0.017	0.014	0.01525
20	4	Seatstay axial	-0.004	0.002	-0.002	0.002	-0.0005
20	5	Chainstay axial	0.027	0.027	0.032	0.027	0.02825

40	1	Top tube	-0.015	-0.01	-0.012		-0.0123333
40	2	Downtube	0.003	0.003	0.003		0.003
40	3	Seatstay hoop	0.017	0.022	0.017		0.018666667
40	4	Seatstay axial	-0.016	-0.013	-0.013		-0.014
40	5	Chainstay axial	0.05	0.052	0.048		0.05
60	1	Top tube	-0.023	-0.024	-0.023		-0.0233333
60	2	Downtube	0.007	0	0.002		0.003
60	3	Seatstay hoop	0.015	0.013	0.01		0.012666667
60	4	Seatstay axial	-0.008	-0.004	0.001		-0.00366667
60	5	Chainstay axial	0.069	0.07	0.071		0.07
65	1	Top tube	-0.014	-0.027			-0.0205
65	2	Downtube	0.012	0			0.006
65	3	Seatstay hoop	0.012	0.01			0.011
65	4	Seatstay axial	0.004	0			0.002
65	5	Chainstay axial	0.072	0.074			0.073
70	1	Top tube	-0.025	-0.031			-0.028
70	2	Downtube	0.007	0.002			0.0045
70	3	Seatstay hoop	0.011	0.01			0.0105
70	4	Seatstay axial	-0.001	0			-0.0005
70	5	Chainstay axial	0.081	0.081			0.081
75	1	Top tube	-0.029	-0.025	-0.029		-0.0276667
75	2	Downtube	0.003	0.005	0.002		0.00333333
75	3	Seatstay hoop	0.007	0.009	0.007		0.007666667

75	4	Seatstay axial	0.007	0.01	0.012		0.009666667
75	5	Chainstay axial	0.089	0.088	0.087		0.088
80	1	Top tube	-0.033	-0.033	-0.03		-0.032
80	2	Downtube	0.001	0.006	0.012		0.00633333
80	3	Seatstay hoop	0.004	0.002	-0.001		0.001666667
80	4	Seatstay axial	0.009	0.013	0.014		0.012
80	5	Chainstay axial	0.108	0.109	0.104		0.107
85	1	Top tube	-0.036	-0.035			-0.0355
85	2	Downtube	0.005	0			0.0025
85	3	Seatstay hoop	-0.007	0			-0.0035
85	4	Seatstay axial	0.026	0.03			0.028
85	5	Chainstay axial	0.118	0.12			0.119

7.3 Redesign Mass and Volume Analysis.

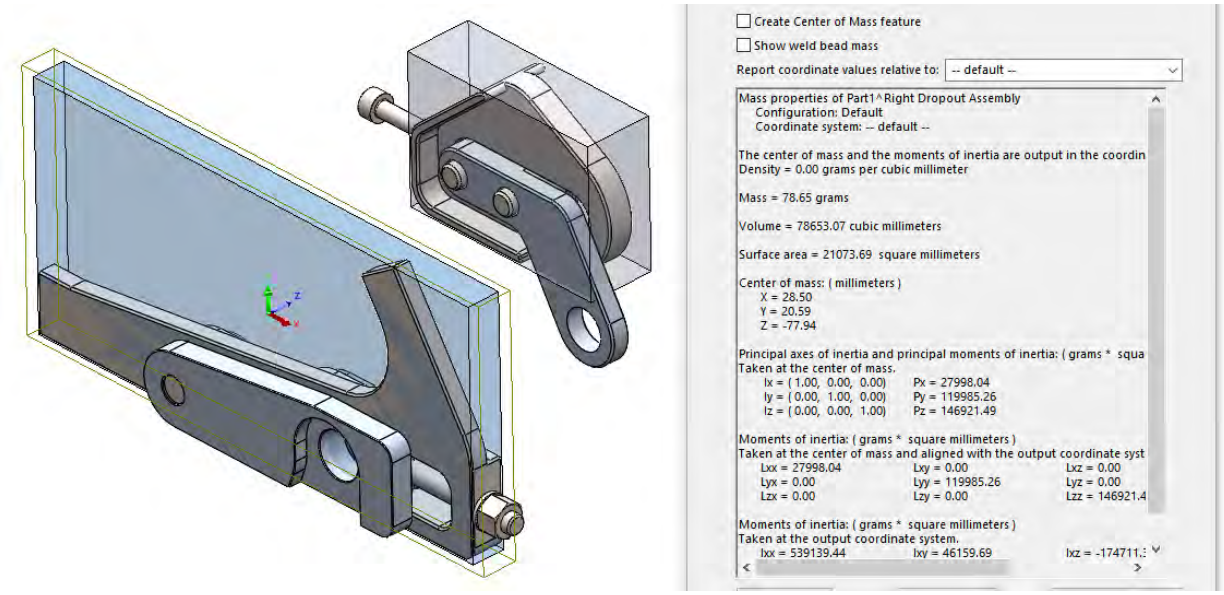

Figure 44: Mass properties of the pre-machined raw material for the current main dropout plate.

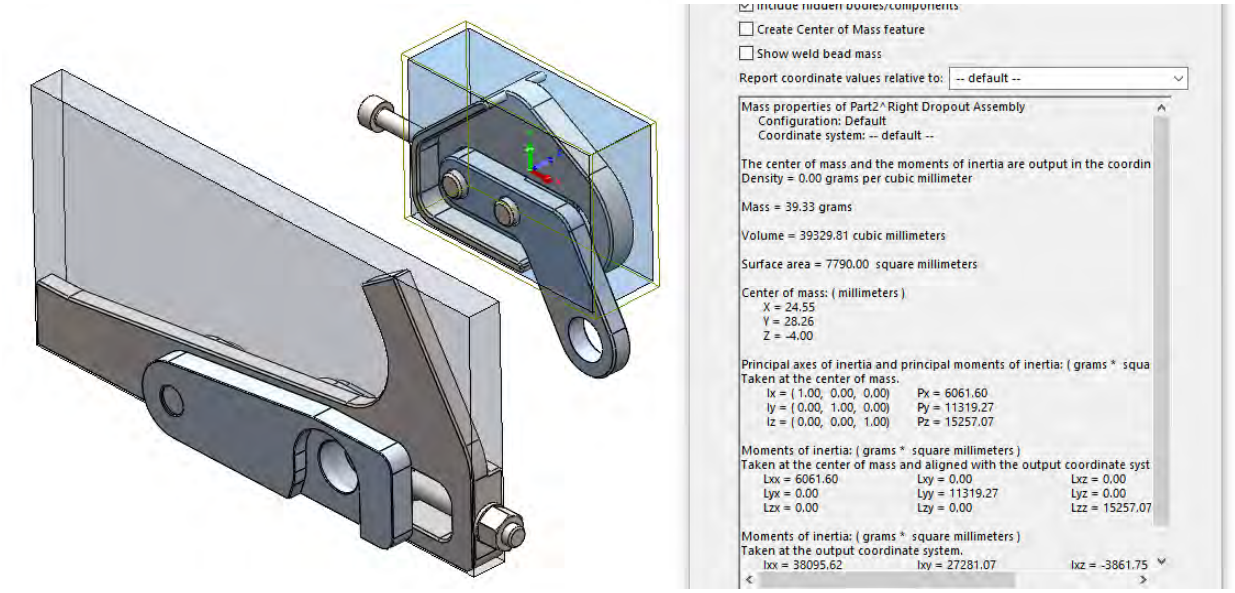

Figure 45: Mass properties of pre-machined raw material for the redesigned dropout plate.

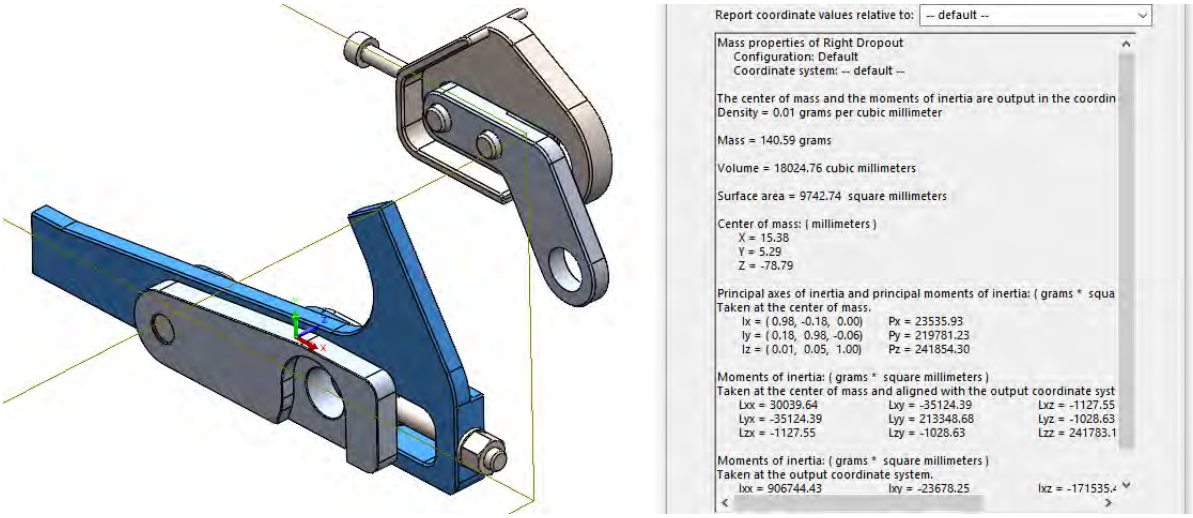

Figure 46: Mass properties of the main dropout plate in the current design.

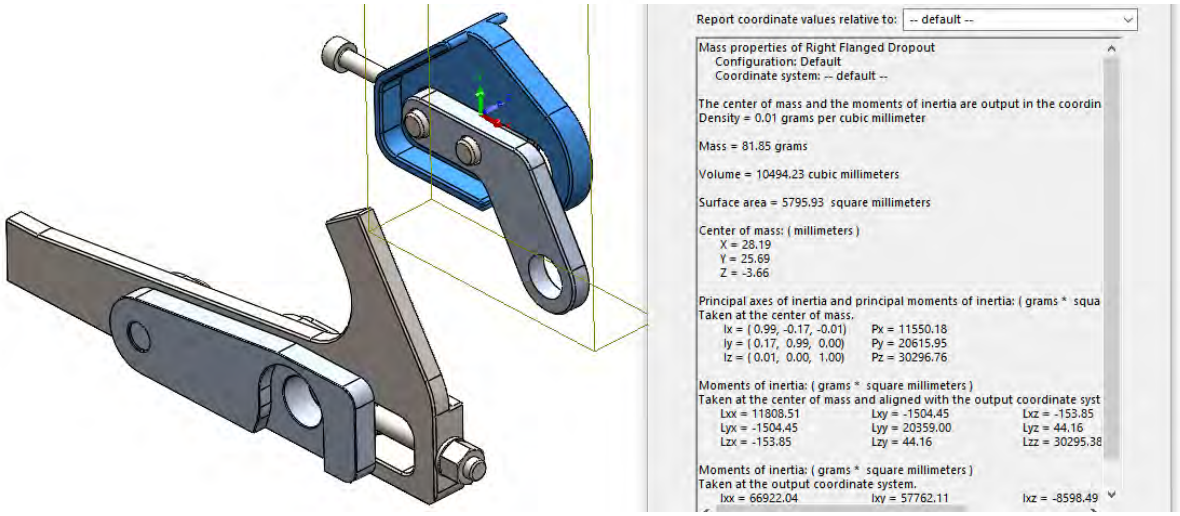

Figure 47: Mass properties of the main dropout plate in the redesign.